Astron. Astrophys. 349, 553–572 (1999)

ASTRONOMY AND ASTROPHYSICS

Galactic B-supergiants: A non-LTE model atmosphere analysis to estimate atmospheric parameters and chemical compositions

N.D. McErlean[1], **D.J. Lennon**[2], **and P.L. Dufton**[1,⋆]

[1] The Department of Pure and Applied Physics, The Queen's University of Belfast, Belfast BT7 1NN, Ireland
[2] Isaac Newton Group of Telescopes, Apartado de Correos 368, E-38700 Santa Cruz de La Palma, Canary Islands, Spain

Received 25 March 1999 / Accepted 13 July 1999

Abstract. A non-LTE model atmosphere analysis of moderate resolution ($R \sim 5\,000$) spectra of 46 Galactic B-type supergiants is presented. Standard techniques are adopted, viz. plane-parallel geometry and radiative and hydrostatic equilibrium. Spectroscopic atmospheric parameters ($T_{\rm eff}$, $\log g$ & $v_{\rm turb}$) and chemical abundances (He, C, N, O, Mg & Si) are estimated, both as a test of the validity of such an approach and in an attempt to provide *consistent* results for supergiants covering a significant range of spectral types.

The values of the estimated atmospheric parameters and their dependence on the physics adopted in the model atmospheres calculations are discussed. The absolute metal abundances are compared to those of main sequence B-type stars and, in general, their chemical compositions appear to be similar. The abundances for He, C, N & O are considered in some detail and are discussed in the context of possible evolutionary histories for this stellar sample.

Specifically, it is found that the supergiant sample can be subdivided into a number of evolutionarily distinct groups. The lower mass objects are predominantly chemically near-normal i.e. their photospheres show little or no evidence for chemical processing, whereas the higher mass supergiants have CNO ratios which are indicative of CN and possibly NO-cycle burning. An attempt is made to quantify the difference in nitrogen and carbon abundances between the high and low mass targets but this is hampered by theoretical uncertainties. The possibilities that the most highly processed supergiants may have either larger rotational velocities or have undergone mass transfer within a binary system are discussed.

Key words: stars: atmospheres – stars: early-type – stars: evolution – stars: supergiants

1. Introduction

In order to understand the chemical evolution of our own and external galaxies, we must have a clear understanding of the evolution of their massive stars. Whilst massive stars constitute only a small fraction of the stellar population within a galaxy, they play an important and fundamental role in its chemical evolution. They are efficient processors of the chemical elements, returning nucleosynthetically enriched material to the interstellar medium (ISM) through stellar winds and supernovae (see, e.g., the review by Maeder & Conti 1994).

Our understanding of the post-main sequence evolution of massive ($M \gtrsim 10 M_{\odot}$) stars is hindered by a number of observational and theoretical uncertainties. Stellar structure calculations (for example, those of Maeder & Meynet 1989 and Schaller et al. 1992) are extremely sensitive to the treatment of convection processes, mass loss and stellar rotation – phenomena which can affect both the evolutionary tracks and, more tangibly, the surface chemistry of such objects. Blue supergiants (BSG) in particular, represent a key challenge to stellar evolutionary theory, as a number of their observed properties remain at odds with current predictions; most notable is their number distribution in the Hertzsprung-Russell diagram – the ratio of blue to red supergiants (RSG) is not reproduced by evolutionary calculations (see Langer & Maeder 1995 and references therein) while the predicted post-main sequence gap at high luminosity is not observed (Tuchman & Wheeler 1990).

An important indicator of evolutionary status is provided by the stellar surface chemistry and considerable qualitative evidence for photospheric chemical peculiarities in luminous stars is available. Jaschek & Jaschek (1967) and later Walborn (1972, 1976) presented evidence for anomalies in the carbon and nitrogen linestrengths in OB stars, leading to the spectral classifications OBN/OBC – analogous to the classifications of Wolf-Rayet stars which were already in use. The OBN/OBC stars have respectively strong/weak nitrogen lines for their spectral type with, in general, the nitrogen variations being negatively correlated with those of carbon; additionally, many stars with only moderate CN anomalies have been identified – thus the morphology may reflect a continuous range of surface chemistries, rather than a strict dichotomy. CNO linestrength anomalies in B-type supergiants are also found in the lower metallicity environments of the Large and Small Magellanic Clouds (Fitzpatrick & Bohannan 1993 and Lennon 1997, respectively).

Such phenomena are broadly supported by current stellar evolutionary theories, which predict that some massive stars

Send offprint requests to: P.Dufton@qub.ac.uk
⋆ On leave of absence at the Isaac Newton Group of Telescopes, Apartado de Correos 368, E-38700, Santa Cruz de La Palma, Canary Islands, Spain

should show variations in their surface abundances indicative of CNO core-processed material being present in the photosphere. However, the mechanism by which such matter is mixed to the stellar surface is still subject to some debate. For example, models by Schaller et al. (1992) imply that some massive stars may evolve through so-called 'blue loops' (main sequence – BSG – RSG – BSG). During their time as RSGs, massive stars develop appreciably enriched photospheres through the convective mixing of core-processed material. After the commencement of core helium burning, the star evolves towards higher effective temperatures once more. Thus, two distinct populations of BSG are postulated – the pre-RSG objects which would be chemically normal and the post-RSG objects which would show evidence of nucleosynthetically processed material having been mixed to their surfaces. Alternatively, Denissenkov (1994) – see also Talon et al. (1997) – has considered the main sequence evolution of a 10 $M_{\odot}$ star, including the effect of rotationally induced turbulent diffusive mixing. He has shown that this important mechanism can provide efficient mixing *during the main sequence lifetime*, thus removing the need for blue loops to explain the OBN/OBC phenomenon.

There is some observational evidence which would favour the latter evolutionary scenario. Schönberner et al. (1988) examined the helium and CNO spectra of 4 late O-type, near main sequence objects, finding substantial changes in their CN abundances, with no evidence for a change in their oxygen abundances. As these effects were accompanied by moderate helium enhancements, they attribute them to *partial* CN-process mixing. This suggests that mixing of core-processed material has occurred on the main sequence. Venn (1995b) considered the CNO abundances of 22 Galactic A-type supergiants, and found N/C ratios which were also consistent with partial mixing having occurred on or near the main sequence.

As well as Schönberner et al., there are a number of authors who have estimated enhanced helium fractions for luminous, early-type stars. Voels et al. (1989), Lennon et al. (1991b), Herrero et al. (1992) and Smith & Howarth (1994) have all found considerable helium enhancements for luminous OB-stars, and in some cases a correlation with CN anomalies. This phenomenon has been referred to as the 'helium discrepancy', as the magnitude of the observed helium enhancements exceeds that predicted by theory. However whilst variations in He I linestrengths are undoubtedly real, they need not necessarily reflect large variations in abundances. McErlean et al. (1998 - hereafter referred to as MLD) have considered the effect of microturbulent line broadening, which was not fully included in the above papers, and for the two representative early B-type supergiants, ϵ & κ Ori, have found lower (and near-normal) helium fractions. If these effects are present in other luminous OB-stars, then published helium enhancements must be considered uncertain. Indeed, Smith & Howarth (1998) have independently shown that the use of microturbulence leads to a near-solar helium fraction in the O9.7 Iab supergiant HD 152003, which lends support to this idea.

The primary motivation of the work presented here was to analyse a statistically significant sample of B-type supergiant spectra in a consistent, quantitative manner and hence to constrain their possible evolutionary histories. In two previous papers (Lennon et al. 1992, 1993 – hereafter referred to as Papers I and II, respectively) a spectral atlas for B-type supergiants was presented together with a tabulation of equivalent width estimates. By examining these data as a function of spectral type, qualitative evidence for variations in their carbon and nitrogen abundances was presented. In this paper, we shall use non-LTE model atmospheres and line formation computations to investigate the physical properties of this sample in a more quantitative manner. Linestrengths will be analysed to yield estimates of absolute, non-LTE abundances and in so doing, we will be able to offer a critique of the uses and limitations of such methods. We will also attempt to quantify variations in the CNO element abundances.

To investigate the possible effect of metallicity, the sample of Galactic supergiants considered here has been supplemented by spectroscopic observations of a further 63 B-type supergiants in the SMC (Lennon 1997); a differential analysis of the two datasets will be presented in a companion paper.

2. Observational data

The optical spectra for the stars listed in Table 1 have been discussed in Papers I and II. In the former paper, details are presented of selection criteria and observing and data reduction techniques, whilst in the latter, equivalent widths of selected lines are tabulated.

Table 1 also presents estimates of each star's distance and luminosity, which are discussed below. Each object has already been assigned membership of a galactic association or open cluster in Paper I. We have taken distance estimates for these stellar aggregates from the literature, using the catalogue of Rupprecht (1966) as a starting point, but using more recent estimates if these were judged to be more reliable. These additional sources were; de Zeeuw et al. (1999) for distance moduli for OB associations and clusters derived from Hipparcos data, the Hipparcos catalogue itself (ESA SP-1200 1997), Massey et al. (1995) for recent spectroscopic parallax results, plus catalogues of Becker & Fenkart (1971), Nicolet (1981) and Humphreys & McElroy (1984). In Paper I the star HD12301 was not assigned membership of any association and we have therefore used the luminosity published by Zorec & Briot (1991) which is derived from a Balmer decrement calibration. We have also reassigned membership of HD213087 from Cep OB1 to Cep OB2, and used the Hipparcos association distance rather than individual Hipparcos distances for all Cep OB2 stars. HD190603 was previously assigned membership of Vul OB2, but upon closer examination it is not obvious which association, if any, this star belongs to. There are stellar aggregates at approximately 1, 2 and 4 kpc in this direction and we have arbitrarily taken a distance of 1.5kpc. Its distance must be considered highly uncertain.

In fact, it should be emphasized that both the distances to individual associations and memberships of those associations are in many cases problematic. As an example we consider HD53138 (o^2 CMa) and HD58350 (η CMa), both of which

were considered secure members of Coll 121. Hipparcos data for Coll 121 was discussed in detail by de Zeeuw et al. (1999) who concluded from parallax and proper motion studies that neither of these stars are members. Per OB1 is another important example, since many of our targets are in this association; we have adopted a distance modulus of 11.9 (corresponding to a parrallax of approximayely 0.4 mas) but two stars (HD13841 and HD13866) have Hipparcos parallaxes of 1.83 and 2.92 mas (though with standard errors of 0.92 and 0.83 mas respectively). We have chosen to adopt a uniform distance for all Per OB1 stars however, since these smaller distances would put these stars on the main-sequence while their spectra are clearly those of supergiants (the extinctions are also consistent with Per OB1 membership). Finally, even the Hipparcos distance of κ Ori of 4.52$\pm$0.77 mas, corresponding to a distance modulus of 6.7, is controversial and should be compared with Hipparcos distance moduli ranging from 7.6 to 8.5 for the different Orion subgroups (Brown et al. 1999).

3. Computation of non-LTE model atmospheres

A grid of non-LTE model atmospheres suitable for the analysis of B-type stars was generated using the code TLUSTY (Hubeny 1988). This grid covered an appropriate range in effective temperature (10 000 K $\leq T_{\rm eff} \leq$ 35 000 K) and included logarithmic gravities from $\log g$ = 4.5 down to near the Eddington stability limit. Models were calculated within the above parameter space, at increments of 2 500 K and 0.25 dex in effective temperature and logarithmic gravity respectively, and for two helium fractions, viz. y = 0.09 (solar) and y = 0.20, where y=N[He]/N[H+He].

The models, which contained only hydrogen and helium, assumed a plane-parallel geometry with both hydrostatic and radiative equilibrium and allow for departures from LTE. In all cases the hydrogen atom consisted of 8 non-LTE levels and the neutral helium atom consisted of 14 non-LTE levels. He I levels having their principal quantum number n = 6, 7, 8 were treated as hydrogenic, levels n = 3, 4, 5 were split into sublevels due to electron spin, but ignored angular momentum, and levels n = 1, 2 were treated fully. Models having effective temperatures greater than 20 000 K also included a He II ion which consisted of 14 non-LTE levels.

The models omit a number of physical effects. The most important is likely to be the lack of metal line-blanketing, but also neglected is the effect of wind-blanketing, whereby increased line opacities in the stellar envelope produces a back-warming effect and a change in the temperature structure through the photosphere. Furthermore, the assumption of a plane-parallel geometry may be of limited validity for the low gravity objects considered here. The consequences of these omissions will be discussed below.

4. Computation of non-LTE line profiles

Line formation calculations were performed using the codes DETAIL and SURFACE (Giddings 1981 and Butler 1984 respectively). DETAIL calculates level populations whilst allowing for departures from LTE, and SURFACE computes the emergent line profiles and fluxes. Such calculations assume that the model atmosphere structure is fixed, and hence may be used to examine second order effects in H/He line formation or to treat impurity elements i.e. the metals. Microturbulent velocities, which are close to the speed of sound, have been found for B-type supergiants. However, this parameter is not well-understood and its magnitude can vary from star to star. Therefore, in the calculation of line profiles, microturbulence has been included as an extra free parameter, and estimates for our sample will be discussed below.

The successful execution of DETAIL & SURFACE over such a large range of atmospheric parameters was not trivial. For these calculations, the model hydrogen and helium atoms were more complex (containing 10 levels of H I, 27 levels of He I and 14 levels of He II), and therefore the first step has been to recalculate the populations using those from the model atmospheres as a starting point. This improvement is important for the computation of line profiles of H I and He I/II and also improves the evaluation of background continuum opacities in the case of the metal lines. In calculating metal ion populations and line-profiles, atomic data were similar to previously published analyses: C II – Eber & Butler (1988), N II – Becker & Butler (1989), O II – Becker & Butler (1988), Si II/III/IV – Becker & Butler (1990) and Mg II – Mihalas (1972). As the model atmospheres do not include metals, LTE populations were used as a starting point.

To realistically compare observed and theoretical line profiles, it is necessary to have reliable estimates of the projected rotational velocities of the stellar sample. Values of $v \sin i$ have been estimated from the metal line profiles as follows; unbroadened Gaussian profiles having equivalent widths which match the observed widths of prominent metal-line features were convolved with a Gaussian function to account for instrumental broadening, and a rotational broadening function (see Lennon et al. 1991a for more details). The amount of rotational broadening was varied until reasonable agreement with the observed profile was achieved. Typically three prominent metallic features were used for each star, with different features offering reasonable internal consistency. The estimates of $v \sin i$, which are included in Table 1, do not include the effects of macro- and microturbulence; hence, they should be considered as upper limits.

4.1. Convergence problems associated with low gravity models

Significant difficulties were encountered in running DETAIL and SURFACE for the silicon model ion at the lowest gravities. For models with effective temperatures greater than that for the peak in Si III linestrength (i.e. $\sim$ 25 000 K), convergence could only be achieved by performing preliminary runs where the resonant transitions of Si III & Si IV were set into radiative detailed balance. The resultant populations were then used as starting points in runs which treated the silicon ions fully, which led to convergence in all cases.

Having successfully converged all silicon populations throughout the grid, the silicon line profiles at 4128, 4131 (Si II), 4552, 4567, 4575, 4813, 4820, 4829 (Si III) and 4088, 4116 Å (Si IV) were computed. However an examination of the line profiles showed that for the lowest gravity models having $T_{\rm eff} \gtrsim 22\,500$ K, significant difficulties remain. For any given effective temperature, the Si III linestrengths would be expected to increase with decreasing logarithmic gravity and indeed this occurred in most cases. However, in models having the lowest gravities, the linestrengths in both Si III multiplets decreased. Examination of the line profiles indicated that this was caused by either emission or 'filling in' of the profiles. Indeed the DETAIL calculations showed an overpopulation of the upper levels in the atmospheric regions where the lines were formed. This was coupled with large photoionisation rates (and subsequent cascades) in these low density models. We do not believe that this effect is real as it leads to anomalous effective temperature estimates compared with other methods (e.g. the He II profiles). Rather, we postulate that the emission is an artefact of our exclusion of line blanketing which leads to an overestimate of the UV flux and hence an overestimate of the photoionisation rates. At these temperatures, the weaker Si III multiplet near 4813 Å, appears to be more reliably modelled than the multiplet near 4552 Å, as it is formed deeper in the atmosphere and is thus less affected by low particle densities and departures from LTE. Indeed its linestrengths appear well-behaved for effective temperatures up to 25 000 K.

The problems which were encountered in the synthesis of the silicon features also seem to be present (but to a lesser extent) in the other elements, where they manifest themselves as chemical abundance anomalies in certain lines. These difficulties, which may be symptomatic of unblanketed, non-LTE models at high effective temperatures and low gravities are discussed further below.

5. Determination of atmospheric parameters

The estimation of reliable atmospheric parameters for B-type supergiants is more fraught than for their main sequence counterparts. Photometric calibrations (such as those of Lester et al. 1986), which rely on the temperature dependence of the Balmer discontinuity, are useful for B-type dwarfs but are inappropriate here as they are generally based upon flux distributions calculated from the LTE model atmospheres of Kurucz (1979, 1991). A further problem is that such methods often neglect the gravity dependence of the stellar continuum, as they are calibrated using the spectra of near main sequence objects. Hence they may not fully account for the redder surface colours produced by the spherically extended supergiant atmospheres.

However, *spectroscopic* methods which allow for non-LTE effects, offer a possible alternative. There are a number of elements observed in B-type supergiant optical spectra which show more than one ionisation stage. For example, ionisation balances due to He I/II, Si III/IV and Si II/III are available as indicators of stellar effective temperature. A number of these spectroscopic indicators has been used, and the estimation of each of the atmospheric parameters are discussed separately below, with results listed in Table 1. As an example, Fig. 1 shows how the atmospheric parameters for χ Aurigae (B4 Iab) were estimated. Fits to the Balmer lines describe a locus in the $T_{\rm eff}$-$\log g$ plane and the subsequent use of a temperature discriminant isolates one single point along this locus which represents the appropriate parameters. In this case the ionisation balance of Si II/III has been performed at three values of $v_{\rm turb}$, and suggests an effective temperature of approximately 16 500 K.

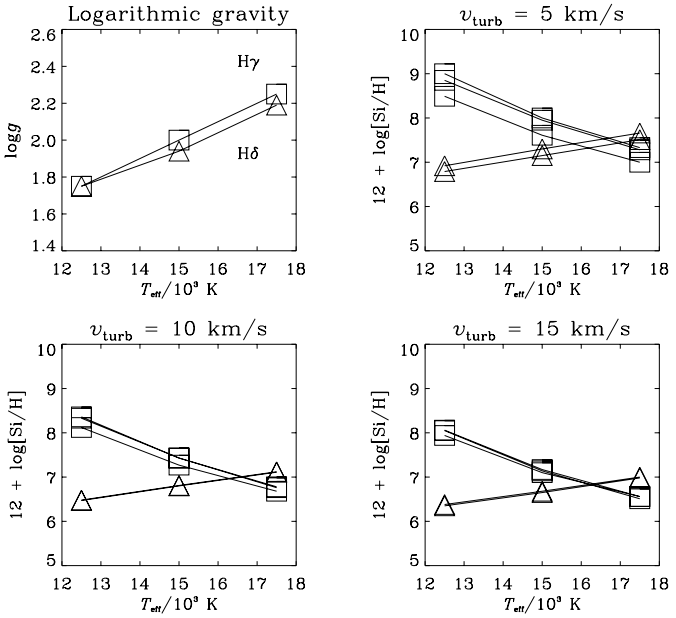

Fig. 1. The estimation of atmospheric parameters for χ Aurigae (B4 Iab). The upper left diagram shows the best fits to H δ and H γ which constrain the allowed values of $\log g$ to the locus used in the other diagrams. The subsequent fits to the Si II/III equivalent widths are shown for three microturbulences (the squares and triangles represent Si III and Si II respectively). These plots suggest an effective temperature of approximately 16 500 K. In this example, $T_{\rm eff}$ is relatively insensitive to $v_{\rm turb}$ as the Si II and Si III linestrengths are similar.

The four atmospheric parameters ($T_{\rm eff}$, $\log g$, y, and $v_{\rm turb}$) are not independent and a degree of iteration is required. The method used – namely the $T_{\rm eff}$-$\log g$ fitting diagram – gave simultaneous estimates for effective temperature and gravity. We have had to consider the possible effects of a varying helium fraction and microturbulence within our sample and our approach has been to initially *assume* a solar helium fraction for all our supergiants. Once the other parameters are estimated, the analysis of the He I lines provides a check on the validity of this assumption. The values estimated for the microturbulence are discussed separately.

5.1. Logarithmic gravity

Tests have shown that the Balmer lines are almost unaffected by microturbulent line-broadening, as they are dominated by both a large Stark effect and a relatively large Doppler broadening due to the high thermal velocities. Hence it was possible to estimate

Table 1. Galactic supergiants and their non-LTE atmospheric parameters. Random errors are typically $\pm 1\,000$ K for $T_{\rm eff}$, ± 0.2 dex for $\log g$, $\pm 20\,{\rm kms}^{-1}$ for $v \sin i$ and $\pm 5\,{\rm kms}^{-1}$ for $v_{\rm turb}^{\rm Si}$. Note that the effective temperatures and logarithmic gravities are based on standard non-LTE techniques and they may not be physically realistic – see text for further discussion. Also listed are the stars' CN status, where $\times$ is 'normal/moderate', $\circ$ is 'processed?' and $\bullet$ is 'highly processed' – see Sect. 7.1. The final two columns contain estimates of distance moduli and luminosities, these are discussed further in Sect. 2.

HD number	Name	Spectral Type	$T_{\rm eff}$ (K)	$\log g$	$v \sin i$ (km s^{-1})	$v_{\rm turb}^{\rm Si}$ (km s^{-1})	CN status	Distance Modulus	Luminosity $\log(L/L_\odot)$
207198		O9 Ib/II	34 000[1]	3.23	80	–	–	8.9	5.05
30614	α Cam	O9.5 Ia	32 500[1]	3.04	100	–	–	9.7	5.60
209975	19 Cep	O9.5 Ib	32 500[1]	3.17	100	–	–	8.9	5.04
167264	15 Sgr	O9.7 Iab	29 000[1]	3.08	100	10	$\circ$	11.3	5.75
37128	ϵ Ori	B0 Ia	28 500[1]	2.94	85	12	$\circ$	8.1	5.50
204172	69 Cyg	B0.2 Ia	28 500[1]	3.02	100	9	$\circ$	9.6	4.47
38771	κ Ori	B0.5 Ia	27 500[1]	3.00	80	12	$\circ$	6.7	4.68
192422		B0.5 Ib	27 000[1]	3.02	90	10	$\circ$	11.4	5.35
213087	26 Cep	B0.5 Ib	26 000[1]	2.92	90	15	$\circ$	8.9	4.83
2905	κ Cas	BC0.7 Ia	*24 000*	*2.70*	80	11	$\times$	10.5	5.61
13854		B1 Iab	23 500[2]	2.64	80	12	$\bullet$	11.9	5.44
24398	ζ Per	B1 Ib	23 000[2]	2.73	60	10	$\times$	7.5	4.90
190603		B1.5 Ia$^+$	21 000[2]	2.35	70	10	$\bullet$	10.9	5.58
14956		B1.5 Ia	21 500[2]	2.49	75	11	$\bullet$	11.9	5.60
13841		B1.5 Ib	22 000[2]	2.70	65	11	$\times$	11.9	4.92
193183		B1.5 Ib	*22 500*	*2.75*	65	10	$\times$	11.4	5.15
41117	χ^2 Ori	B2 Ia	19 500[2]	2.20	65	12	$\bullet$	10.9	5.55
14818	10 Per	B2 Ia	20 000[2]	2.38	70	10	$\bullet$	11.9	5.37
14143		B2 Ia	20 000[2]	2.31	65	11	$\bullet$	11.9	5.43
194279		B2 Ia	19 000[2]	2.15	70	15	$\bullet$	11.2	5.66
206165	9 Cep	B2 Ib	*20 000*	*2.50*	55	15	$\times$	8.9	4.78
13866		BC2 Ib	*20 500*	*2.60*	75	12	$\times$	11.9	4.74
31327		B2 II	21 500[3]	2.90	50	15	$\times$	10.8	5.14
42087	3 Gem	B2.5 Ib	20 500[3]	2.55	60	15	$\times$	10.9	4.96
198478	55 Cyg	B2.5 Ia	18 000[3]	2.18	45	11	$\times$	9.2	4.84
224055		B3 Ia	17 000[3]	2.08	45	15	$\times$	12.7	5.62
225094		B3 Ia	18 000[3]	2.20	60	9	$\times$	11.7	5.12
53138	o^2 CMa	B3 Ia	18 500[3]	2.35	55	10	$\times$	9.5	5.04
14134		B3 Ia	18 000[3]	2.30	60	10	$\times$	11.9	5.35
36371	χ Aur	B4 Iab	16 500[3]	2.15	40	10	$\times$	10.8	5.31
58350	η CMa	B5 Ia	16 000[3]	2.10	40	15	$\times$	10.0	5.36
4841		B5 Ia	14 750[3]	1.95	40	–	$\times$	11.9	5.11
7902		B5 Ib	15 500[3]	2.05	35	–	$\times$	12.2	4.92
164353	67 Oph	B5 II	16 500[3]	2.46	10	–	$\times$	8.2	4.10
191243		B5 II	15 500[3]	2.43	0	–	$\times$	11.7	4.83
15497		B6 Ia	15 000[3]	2.00	35	–	$\times$	11.9	5.28
13267	5 Per	B6 Ia	15 000[3]	2.00	30	–	$\times$	11.8	4.92
12301	53 Cas	B7 II	14 000[3]	2.15	0	–	$\times$	9.4	4.40
199478		B8 Ia	12 500[3]	1.56	45	–	$\times$	11.2	4.89
34085	β Ori	B8 Ia	13 000[3]	1.75	40	–	$\times$	6.9	4.87
14542		B8 Ia	12 500[3]	1.75	45	–	$\times$	11.9	4.87
208501	13 Cep	B8 Ib	13 000[3]	1.80	40	–	–	8.9	4.33
14322		B8 Ib	13 000[3]	1.85	35	–	–	11.9	4.60
21291		B9 Ia	11 500[4]	1.60	10	–	–	9.8	4.88
35600		B9 III	11 000[4]	2.00	0	–	–	10.8	4.31
14899		A0 Ib	11 000[4]	1.75	0	–	–	11.9	4.32

Effective temperatures deduced from
[1] He II profile fits
[2] Si III/Si IV ionisation balance
[3] Si II/Si III ionisation balance
[4] $uvby$ photometry
Temperatures in italics are based on spectral type – see text.

gravities for all supergiants with no prior knowledge of $v_{\rm turb}$. The Balmer lines Hδ and Hγ have been used with a greater weighting being given to the former, as in some stars the core of Hγ was slightly filled by wind emission. However, for the majority of the stars considered here, agreement between the two lines was good.

We have not used fits of Hϵ, which was available in all our spectra, due to blending with an interstellar line of calcium and a stellar He I line. Neither have we considered Hα or Hβ as wind effects can be significant in these lines (see Paper I).

5.2. Effective temperature

The relatively wide range of spectral types in our sample precludes the use of a single temperature indicator. Here, the primary objective was to obtain atmospheric parameters across the large range of spectral types, whilst achieving a reasonable degree of consistency and our approach was as follows:

Late O-type and very early B-type supergiants. Where possible we have used He II features as indicators of effective temperature. It should be noted, however, that a strict ionisation balance has *not* been performed, as other authors have found that the temperature estimates derived in this way are strongly dependent upon of the choice of He I line used (see, for example, Lennon et al. 1991b and Herrero et al. 1992). Indeed, the sensitivity of the He I lines to the adopted microturbulence may be partially responsible for the above inconsistencies in He I/II temperature estimates. Here, we have initially *assumed* a normal helium fraction, and having determined the locus of suitable $\log g$ values from the Balmer lines, have estimated effective temperatures by fitting the profiles of the He II lines alone.

It has been shown by MLD that the He II lines at 4200 and 4542 Å are almost unaffected by microturbulence at temperatures appropriate to early B-type supergiants. The He II line at 4686 Å was not used as it is strongly affected by stellar winds, as shown by Gabler et al. (1989). He II 4200 Å is blended with a N III feature and hence a greater weight was given to the line at 4542 Å.

Early B-type supergiants. For those objects having spectral types from B0 to B2, strong features due to Si III and Si IV were simultaneously observed. However, as was discussed in Sect. 4.1, the stronger Si III features are not well modelled for the low gravity models at effective temperatures greater than approximately 25 000 K (while discrepancies may well extend to lower temperatures). Hence, the weak Si III multiplet near Hβ was used in conjunction with the Si IV feature near 4116 Å in order to obtain the effective temperature at which the predicted abundances from the two ionisation stages matched. The synthetic silicon profiles computed from the lowest gravity models have been rejected in favour of a modest extrapolation (over less than 0.25 dex) from the more reliable, higher gravity models. The luminosity class II/Ib objects in this spectral type range (whose silicon lines appear to be well modelled) have effective temperatures which support the validity of this approach.

The strengths of these lines are dependent on the microturbulent velocity and hence ionisation balances were performed for $v_{\rm turb}$ = 5, 10 & 15 kms^{-1}. In most cases the temperature estimates were relatively insensitive to $v_{\rm turb}$. The largest effects were (as expected) at spectral types where the line strengths from the two ionisation stages were significantly different. However, even then the effect was small and a subsequent estimation of $v_{\rm turb}$ allowed the effective temperature to be unambiguously defined.

Mid and late B-type supergiants. For supergiants of spectral type later than approximately B2.5, strong absorption features due to Si II and Si III are observed. At the lower effective temperatures applicable to these objects, the silicon lines are believed to be well modelled and hence it was possible to assign each star a temperature based on the ionisation balance of the features at 4552/4567/4574Å (Si III) and 4128/4131 Å (Si II). Again microturbulent velocities between 5 and 15 kms^{-1} were considered.

Using the temperature indicators listed above allowed the estimation of atmospheric parameters for 39 out of the 46 target stars. For four of the remaining objects (κ Cas, HD 193183, 9 Cep & HD 13866) effective temperatures were adopted based on those found for other stars with the same spectral type – logarithmic gravities were still available from the fits to H δ/H γ. As these objects occupy small 'gaps' in our spectral type-$T_{\rm eff}$ scale, this should not lead to significant error.

However, the three objects having the latest spectral types in our sample have no spectroscopic temperature indicators. In these cases we have used Strömgren $uvby$ photometry (obtained from the General Catalogue of Photometric Data – see Mermilliod et al. 1997) and the calibration of Lester et al. (1986). As discussed above, the temperature scales of the Kurucz line-blanketed model atmospheres and those used here may not necessarily be the same. Hence, photometric temperatures were assigned to the bottom 10 stars in the list. Those having effective temperatures from both spectroscopic and photometric indicators suggest that, at around spectral types B6-B8, the two scales *are* similar. Hence, we have adopted the photometric temperatures for the three coolest stars. Whilst this may lead to inconsistencies with the rest of the sample, the errors are likely to be small and should not affect the main conclusions of this paper, which are principally based on the stars of spectral type earlier than B7.

5.3. The microturbulent velocity, $v_{\rm turb}$

Previous work on luminous blue stars has consistently produced rather large values for the microturbulent velocity. Lennon et al. (1991b) analysed three B0.5 Ia supergiants (in the Galaxy, the LMC and the SMC respectively) using non-LTE techniques similar to those used here, and they adopted a value of $v_{\rm turb}$ = 10 km s^{-1}, noting however that this value was not sufficiently

large to remove the slope in abundance. Gies & Lambert (1992) analysed a large number of B-type stars, of which three were supergiants, in both LTE and non-LTE. They found for their supergiants, that by assuming LTE a high value of $v_{\rm turb}$ $\sim$30 km s^{-1} was obtained, and that by moving to a non-LTE analysis, this value was reduced to $v_{\rm turb}$ $\sim$15 kms^{-1}. More recently Smartt et al. (1997) analysed the spectra of four supergiants near the Galactic Centre using both LTE and non-LTE techniques and in both cases deduced microturbulences of $\sim$ 30 kms^{-1}.

MLD have shown that in the case of the early B-type supergiants ϵ & κ Ori (also analysed in this work), the lines of Si III indicate a smaller microturbulence than do the lines of O II ($v_{\rm turb}^{\rm Si\,III}$ $\sim$ 12 kms^{-1} as compared to $v_{\rm turb}^{\rm O\,II}$ $\sim$ 30 kms^{-1}) – this effect has been independently discovered by Vrancken (1998) in her analyses of early B-type giants in h & χ Persei. Whilst O II has the advantage that it shows many absorption lines with a great range in equivalent width, the Si III lines at 4552, 4567 & 4574 Å offer a reasonable range in linestrength and are from the *same multiplet*. Hence they are likely to be less affected by such problems as errors in the atomic data and the inadequate treatment of non-LTE effects. For these reasons, the Si III lines have been used to estimate microturbulent velocities where possible and these are listed in Table 1.

By using the Si III features, microturbulences have been estimated for supergiants having spectral types between approximately B0 and B5. Within this range in effective temperature, $v_{\rm turb}$ seems to remain essentially constant at 10–15 kms^{-1} and there seems little dependence on luminosity class (to within the errors). There is some tentative evidence that this value may decline for later spectral types, as the ionisation balance diagrams provide some indication of the appropriate microturbulence. For example, in the case of χ Aurigae (see Fig. 1), the 'tightness' of the lines suggests that $v_{\rm turb}$ $\sim$ 10–15 km s^{-1} may be appropriate. For stars later than B5, equivalent diagrams indicate that values of between 5 and 10 km s^{-1} may be correct. However, at these temperatures the Si III lines are weak and hence are both less reliably measured and have a smaller dependence on $v_{\rm turb}$. Therefore, the information on microturbulence is essentially derived from the Si II features which have very similar linestrengths. Unfortunately, other suitable spectral indicators for the microturbulent velocity were not available at these spectral types. Whilst the suggestion that $v_{\rm turb}$ may decline towards $\sim$ 5 km s^{-1} for late B-type supergiants is a tentative one, it *is* in agreement with the work of others; for example, Venn (1995a) finds LTE microturbulences of 5–8 kms^{-1} for her A-type supergiants.

For the analyses of element abundances which follow, the value $v_{\rm turb}$ = 10 km s^{-1} has been assumed throughout. It is possible that $v_{\rm turb}$ may be a function of effective temperature or of gravity and any errors present in our analysis due to this simplification will be considered below.

6. Results

As this paper represents a first attempt to assign purely non-LTE atmospheric parameters to a large sample of B-type supergiants in a self-consistent and purely spectroscopic manner, we shall preface our results on chemical abundances with a discussion of the estimated atmospheric parameters. We shall compare our results (in particular the effective temperature scale) to the results published by other authors and shall discuss the errors, both systematic and random, which are present in our methods.

Because of the rather large number of supergiants in our dataset and the moderate quality of the spectroscopic data, we shall not attempt to chemically analyse each star independently. We shall instead examine the variations in linestrength as a function of effective temperature with the following aims:–

- To investigate whether standard non-LTE methods can adequately reproduce the spectra of B-type supergiants.
- Subject to the above, to estimate the non-LTE absolute abundances of the sample as a whole.
- To quantify the linestrength variations in terms of abundance depletions or enrichments, focussing principally on those elements which are indicative of the presence of core-processed material in the photosphere.

6.1. Atmospheric parameters

Any chemical analysis depends upon the the reliability of the estimated atmospheric parameters, in particular that of the effective temperature scale ($T_{\rm eff}$). Many authors have ascribed temperature scales to early-type stars using a variety of empirical and more theoretical methods – a recent review is given by Crowther (1997). As well as the random errors associated with, e.g., errors in equivalent width measurements or line profile fitting, there are systematic offsets between the different scales due to the differing physical assumptions inherent in each method.

The $T_{\rm eff}$-$\log g$ estimates, which are listed in Table 1, are reproduced in graphical form in the upper panel of Fig. 2. Also shown, in the lower panel, is a comparison of the $T_{\rm eff}$-scale derived here with the effective temperature versus spectral type scale used in Paper II, which was based upon that used by Barlow & Cohen (1977) and Lamers (1981). We emphasise that the temperature scale will be strongly dependent on the method used to obtain it. In particular the treatment of non-LTE effects and of line blocking may have significant effects. It is immediately apparent from the lower panel that the $T_{\rm eff}$-scale derived here is systematically hotter than that used in Paper II. This difference may be at least partly due to the lack of metal line-blocking in our non-LTE models and is not unexpected. However, whilst the systematic differences are real, they are probably not important for this analysis – the important point is that a *consistent* scale is used throughout.

Despite the problems in applying Kurucz's LTE model atmospheres (1979, 1991) in the analysis of luminous stars such as are considered here, the Kurucz temperature scale is likely to be more physically realistic and closer to the empirical scale due to the fuller treatment of metal line blocking. Certainly, in the analysis of main sequence B-type stars, the Kurucz scale has been widely used (see, for example, Hibbins et al. 1998 and Smartt et al. 1996a, 1996b) and it would be useful to compare

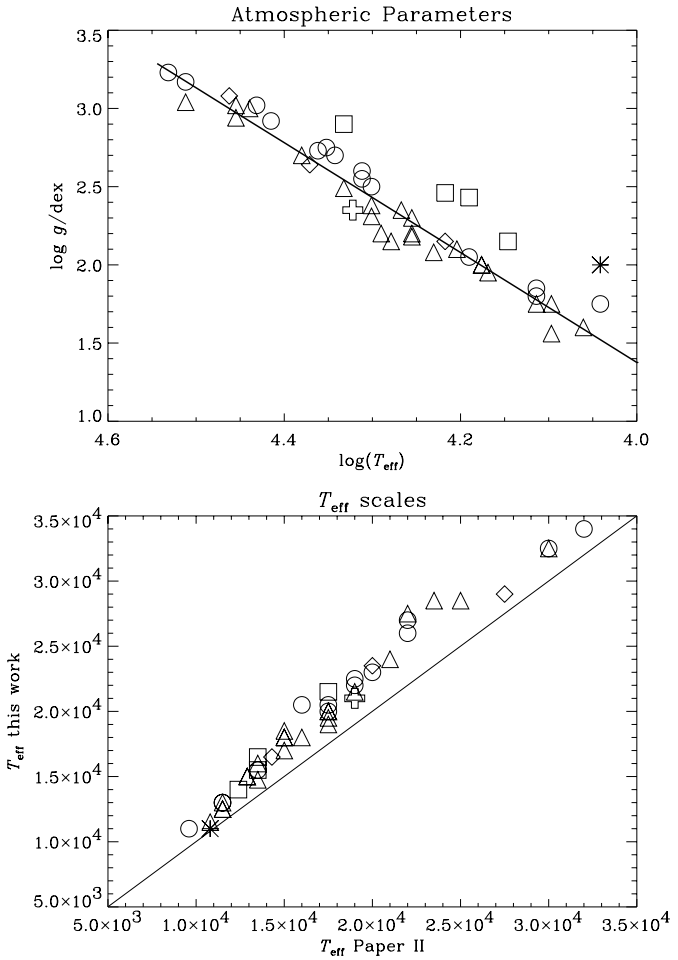

Fig. 2. Top: The estimated values of effective temperature and logarithmic gravity – as listed in Table 1. The symbols refer to the luminosity class as follows: cross – Ia$^+$, triangle – Ia, diamond – Iab, circle – Ib, box – II and asterisk – III. Also shown is a linear fit, which excludes the luminosity class II and III objects. This fit then represents the *average* atmospheric parameters of the supergiant sample. **Bottom:** A comparison between the $T_{\rm eff}$-scale estimated here and that adopted in Paper II – see text for further discussion.

our scale with it. Recent analyses of early B-type supergiants (Smartt 1996) using both blanketed and unblanketed techniques have shown that the latter yield $T_{\rm eff}$ estimates which are typically 10% higher than the former – this relationship has been recently confirmed by Hubeny et al. (1998) at higher effective temperatures.

In order to further investigate and confirm this relationship, we have examined the temperature-optical depth structures of our models and those of Kurucz. The aim is to derive a mapping between the temperature scale of Kurucz and that of our non-LTE unblanketed models. However, the task is made significantly more difficult as the gravity label of a model atmosphere may also depend on the physics included in the model. It has been shown recently (Lanz et al. 1996) that the derived stellar gravity may change significantly depending on whether or not line blocking is treated. Thus the correct mapping may not be purely along the temperature axis, but may also have a component in the $\log g$ direction. The situation is further complicated as achieving convergence with Kurucz models at low gravities (such as may be appropriate for the supergiants analysed here) can be very difficult. For this reason, our grid of Kurucz models does not go to as low gravities as our TLUSTY grid. Hence, it would be a non-trivial effort to fully determine the nature of the mapping between the two scales, if such a simple relationship exists, and we have not attempted to rigorously define such a mapping.

However at gravities appropriate to (near) main-sequence stars ($\log g$ = 4.0), a shift in effective temperature of approximately 10% yields reasonable agreement between the temperatures in the line forming region – the sense of this shift in going from the TLUSTY scale to the Kurucz scale is a decrease in the effective temperature label of the corresponding model. Whether this shift can be assumed to be appropriate for supergiants is unclear. The situation is complicated further by the possible effect of a stellar wind on the Balmer line profiles, which might lead to a further error in our estimated gravities. For these reasons, we tentatively suggest that a reduction of approximately 10% in our $T_{\rm eff}$-scale may be appropriate to allow for the effects of line blanketing.

A clear separation between the luminosity classes is evident in the upper panel of Fig. 2. In particular, the luminosity class II/III objects are distinct from the other supergiants. For example, a large range in gravity is present at $\log T_{\rm eff} \sim 4.3$ (spectral type B2 on our scale) and simply reflects the increased range in luminosity classes observed at this spectral type. There is also evidence that effective temperature is a function of gravity at fixed spectral type, in the sense that stars having lower gravities also have lower $T_{\rm eff}$ (see Table 1). This 'shear' effect has been examined by Voels et al. (1989) for a sequence of stars having spectral type O9.5, who found a monotonic dependence of $T_{\rm eff}$ on $\log g$ – for Ia to V; $T_{\rm eff}$ = 30 000 K to 35 000 K – in qualitative agreement with our results.

In the syntheses of helium and metal line linestrengths, the effect of these gravity variations has been included in the following manner: The straight line in Fig. 2 (upper panel) shows a least-squares fit through the $T_{\rm eff}$-$\log g$ plane – this fit excludes the luminosity class II & III objects and hence represents the *average* parameters of the luminous supergiant sample. In generating theoretical linestrengths as a function of $T_{\rm eff}$, we have used the appropriate $\log g$ values given by this fit. Thus, the loci of non-LTE linestrengths which are used below, might be expected to reproduce the general behaviour of the spectral features as a function of temperature, but will not allow for any variations in the gravity of individual stars from this least squares fit.

6.2. Helium fractions, y

In Fig. 3 the observed and predicted strengths of He I lines are compared. The singlet and triplet series lines (in order of increasing oscillator strength) are shown on the left and right respectively, for two helium fractions, y = 0.09 (solar) and y = 0.20. MLD have previously shown that it is important to use a non-zero microturbulence when modelling these features in

early B-type supergiant spectra. Hence in order to confirm this conclusion, we included non-LTE results for two values of the microturbulent velocity, $v_{\rm turb}$ = 0, 10 km s^{-1}.

From inspection of Fig. 3, it is obvious that there are a number of unresolved problems in reproducing the He I spectra of B-type supergiants. Considering first the question of microturbulence, we confirm our previous finding that a non-zero value for $v_{\rm turb}$ leads to improved agreement between theory and observation – this improvement is apparent in all lines except 4437 Å (the weakest line under consideration here). In all cases, the trivial result is found that using an increased microturbulence leads to a reduction in the estimated value of the helium fraction and apart from the line at 4437 Å, this brings the y-estimates closer to the solar value. The effect is most obvious, perhaps, in the cases of the lines at 4471 Å and 4713 Å (both triplets), which for $v_{\rm turb}$ = 0 km s^{-1} imply that a helium fraction, $y > 0.2$, for most of the supergiant sample. More importantly, as was shown by MLD, microturbulent line broadening leads to an improvement in the quality of the He I line profile fits.

The neutral helium lines may be subject to the 'generalised dilution effect' (as discussed by Voels et al. 1989), whereby various He I level populations are enhanced due to sphericity, leading to a strengthening of the triplet lines relative to the singlets. Voels et al. suggested that the He I lines forming deepest in the atmosphere should be least affected and should therefore provide more reliable y-estimates. This logic has been used by a number of other authors (e.g. Smith & Howarth 1994) and it is noticeable that these papers estimate smaller helium fractions than those which use all available He I lines (e.g. Lennon et al. 1991b). As formation depth is primarily determined by the intrinsic strength of the line, the weakest lines should be the more reliable. Indeed, Fig. 3 does seem to confirm this result – the singlet and triplet systems *do* suggest that the estimated y-value increases with oscillator strength.

Finally, as was noted by MLD, the triplet lines appear to indicate higher helium fractions than the singlets. In the above paper this was attributed to the lack of metal line blocking, which leads to a spurious calculation of the ultraviolet radiation field. As has been discussed by Lennon & Dufton (1989), this could be particularly important in calculating the photoionisation rates from the n=2 levels in He I, especially for the metastable 2^3S state – it is unlikely to be as important for photoionisation from the ground state, as the flux in this spectral region for B-type supergiants is very low. This may explain the well-known difficulties in reproducing the triplet features at 5876 and 10 830 Å in non-LTE calculations such as these. If this hypothesis were correct, we might expect that the problem would be less important for the late B-type supergiants due to the reduced flux in the n = 2 continua of He I and there is tentative evidence that this is the case (e.g. the 4471 Å line). In any case, the singlet lines seem to be more reliably modelled over the whole temperature range, with the line at 4387 Å giving the most satisfactory fits.

Given the problems associated with modelling the lines of He I, it is difficult to unambiguously identify any supergiants which may be helium rich. The dependence of the linestrengths on gravity, which is not explicitly included in Fig. 3, is an added complication. It seems that the only reliable way to examine the helium fractions is to perform individual examinations of the line profiles, which is beyond the scope of this paper. However, we will further discuss the possibility of a variation in helium fraction in our sample below.

6.3. Absolute metal abundances

As was explained above, we shall not give absolute elemental abundances for individual objects in our supergiant sample, but shall instead give a broader based analysis of the targets as a whole. Such an approach requires that we make comparisons with previously published abundances in early-type stars. However, the different analytical methods which have been used and the sensitivity of the results to such methods mean that it is not immediately obvious which analyses represent the most suitable comparisons. We shall therefore begin with a discussion of recent abundance analyses performed on B-type stars, limiting our discussion to those analyses which used non-LTE techniques applied to optical spectra.

Gies & Lambert (1992) and also Cunha & Lambert (1992, 1994) have examined a significant number of B-type stars and give pseudo-non-LTE abundances. The overlap between their work and ours is somewhat limited in the sense that their target lists comprise mostly main sequence or near main sequence objects and only include a small number of B-type supergiants. They have also concentrated on objects in the spectral type range B0-B3 (which covers the peaks in strength of lines due to CNO). However, each of their papers uses a consistent (and reliable) philosophy in obtaining abundances – essentially an LTE methodology. In obtaining the atmospheric parameters (effective temperature and gravity), they have used profile fits to the pressure-sensitive Balmer lines (typically H γ) and a published calibration of the temperature-sensitive [c_1] photometric index. They derive LTE atmospheric parameters and element abundances and then use a sophisticated mapping procedure to allow for non-LTE effects in individual lines. Aside from the limited overlap between their stellar sample and ours, their reliance on 'photometric' temperatures, which use Kurucz's LTE model fluxes as a calibration, may mean that their work does not provide suitable material for comparison with our results which omit the effect of line-blocking and use ionisation equilibria as the temperature indicator.

In a series of recent papers, Kilian has also made substantial efforts in the area of non-LTE B-type star abundance estimations (see Kilian 1992, 1994 and references therein). Again, her sample primarily consists of near main sequence objects. However, her non-LTE methods are very similar to those used here – her spectroscopic approach in estimating atmospheric parameters (Kilian 1991) and non-LTE philosophy is closely mirrored by ours. Kilian has used the LTE line-blanketed model atmosphere structures of Gold (1984), but her treatment of the non-LTE problem is similar to ours in that line blocking is not treated in her statistical equilibrium and line transfer computations. Of particular importance is that our atomic datasets are effectively identical to those used by Kilian. Therefore, whilst differences

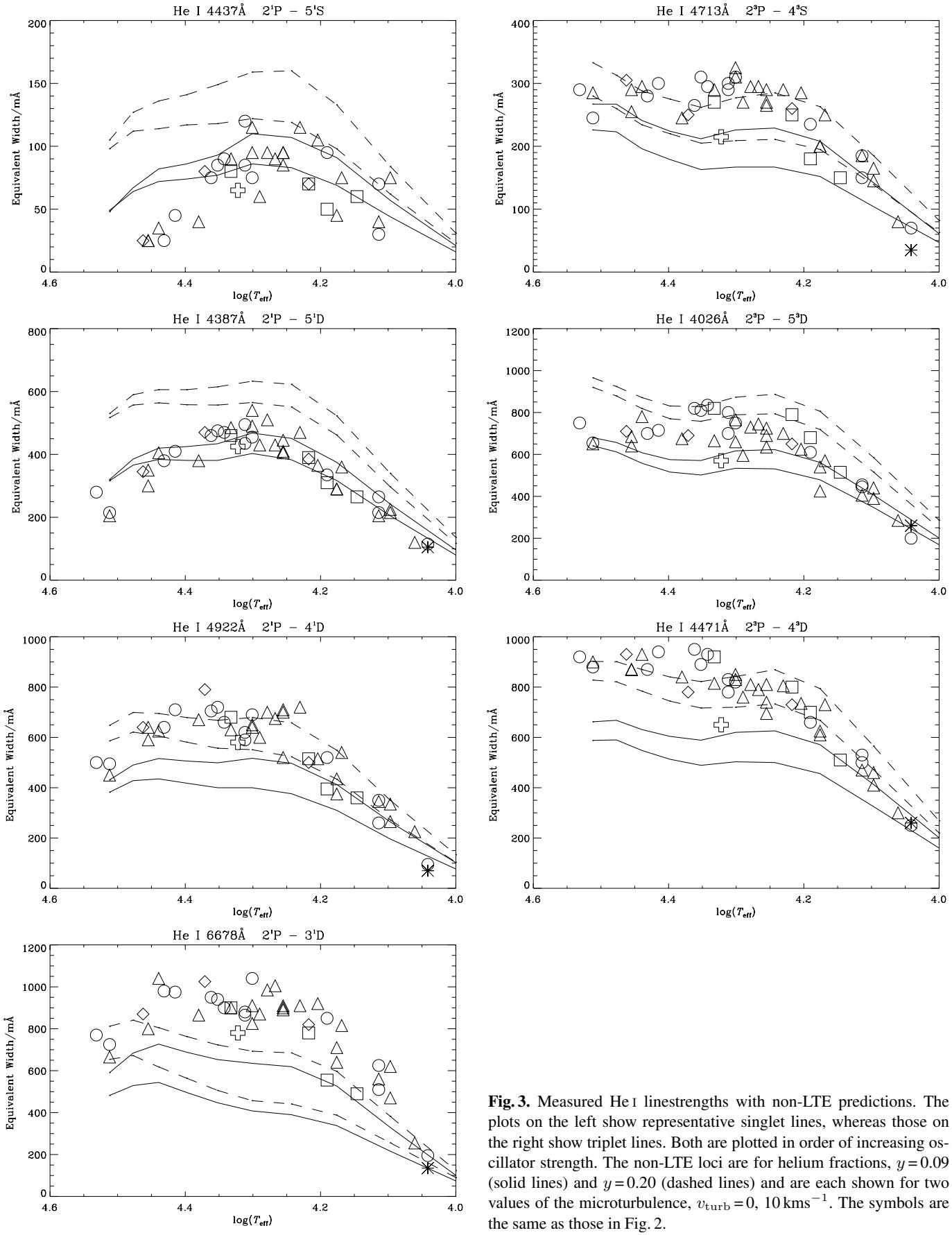

Fig. 3. Measured He I linestrengths with non-LTE predictions. The plots on the left show representative singlet lines, whereas those on the right show triplet lines. Both are plotted in order of increasing oscillator strength. The non-LTE loci are for helium fractions, $y = 0.09$ (solid lines) and $y = 0.20$ (dashed lines) and are each shown for two values of the microturbulence, $v_{\rm turb} = 0$, 10 kms^{-1}. The symbols are the same as those in Fig. 2.

Table 2. Mean non-LTE abundances for main sequence B-type stars (on the logarithmic scale with hydrogen being 12), as compiled from the work of Kilian. Also shown are the number of stars used in determining the average, n, and the standard deviation in the mean, σ (see text for further details).

Element	Abundance	n	σ
C II	8.20	19	0.09
N II	7.69	17	0.15
O II	8.55	20	0.10
Si II/III/IV	7.28	16	0.11
Mg II	7.38	20	0.12

are likely between the $T_{\rm eff}$-scale derived by Kilian and that derived here, element abundances are likely to be comparable. For these reasons we have elected to compile representative non-LTE B-type main sequence stellar abundances from the results of Kilian.

Within her sample of 21 near main sequence B-type stars, Kilian identifies three stars as having anomalously high nitrogen abundances and four stars as having anomalously low silicon abundances. The nitrogen enrichments are attributed to chemical processing effects and the apparent silicon depletions are likely to be due to difficulties in modelling her cooler stars' silicon spectra. In compiling the 'normal' abundances, listed in Table 2, we have excluded these results – our rationale being that we wish to make comparisons with *unprocessed* stellar material. However, the slightly higher value for the standard deviation, σ, in the case of nitrogen may indicate a larger intrinsic scatter in the nitrogen abundances within Kilian's sample.

Rather than discuss the chemical elements in order of their atomic number, as is conventional, we shall deal first with those elements which are likely to have a unique abundance throughout the stellar sample (i.e. Mg & Si). We shall then discuss those elements whose linestrengths may be affected by abundance variations (i.e. CNO).

6.3.1. Magnesium

Our spectral data provided only one feature due to Mg II, namely the close doublet at 4481 Å, whose observed equivalent widths are shown in Fig. 4. As this line is used as a primary indicator in the spectral typing of B-type stars, any large discontinuities would call our temperature scale into question. Therefore the observed smooth monotonic variation with effective temperature is reassuring. A greater range in observed linestrengths at $\log T_{\rm eff} \sim 4.3$ is most probably due to the larger range in surface gravities at this temperature (see Fig. 2).

Also shown are non-LTE results for the representative B-type stellar magnesium abundance of 7.38 dex (full line) with additional loci at $\pm$0.2 dex – all for $v_{\rm turb}$ = 10 km s^{-1}. Our non-LTE calculations suggest that the abundance for our supergiant sample may be constant at $\sim$ 7.58 dex. This is slightly higher than the magnesium abundance implied by results of Kilian, but the agreement is still relatively good given the different luminosity classes of the two samples.

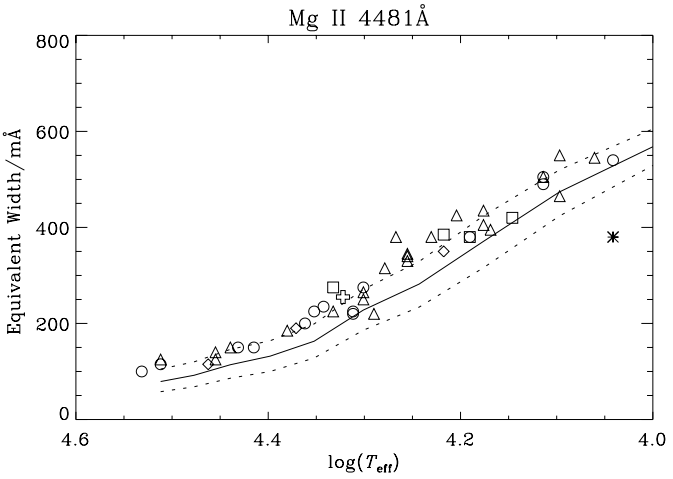

Fig. 4. Observed Mg II equivalent widths compared with the non-LTE predictions. The non-LTE locus is for a magnesium abundance of 7.38 dex with $v_{\rm turb}$ = 10 kms^{-1} (full line). Also shown are loci for magnesium abundances at $\pm$ 0.2 dex (dotted). The symbols are the same as those in Fig. 2.

6.3.2. Silicon

In Paper II, equivalent widths were given for 11 spectral features due to silicon, covering three ionisation stages and 5 multiplets. For Si II, we have elected to show the line at 4128 Å – the other component of this doublet is at 4131 Å and shows a qualitatively similar behaviour. A second doublet was also measured at 6347 & 6371 Å but was not well modelled by our non-LTE computations and has not been included here. There are two multiplets due to Si III which were measured in Paper II, viz. the triplets at 4552, 4567 & 4574 Å and 4813, 4819 & 4829 Å. The second of these multiplets is not illustrated as it is inherently quite weak, while the feature at 4552 Å has been selected as representative of the first multiplet. Only one spectral feature due to Si IV is shown, that is the line at 4116 Å. The other component of this doublet (at 4088 Å) suffers blending problems due to a nearby line of O II.

The observed and predicted equivalent widths for these lines are shown in Fig. 5. The synthetic line strengths are for a silicon abundance of 7.28 dex (with $\pm$0.2 dex) and a microturbulence of 10 km s^{-1}. However, as some difficulties remain with the non-LTE modelling of these lines, the predictions are only plotted for restricted ranges of effective temperature.

The silicon lines are believed to be well modelled in the temperature range where Si II is strong and indeed agreement between theory and observation for the Si II feature is good. There may be a decline (relative to the theoretical calculations) in the observed linestrengths at later spectral types, possibly due to a decrease in the microturbulence in these objects.

The Si III line at 4552 Å is observed from spectral types B0 to approximately B8, but is not well modelled above $T_{\rm eff} \sim$ 22500 K and hence the non-LTE locus in Fig. 5 is restricted. Below this temperature, the feature appears to be predicted well by our non-LTE computations and agreement is excellent. This line is particularly sensitive to gravity and it is interesting to

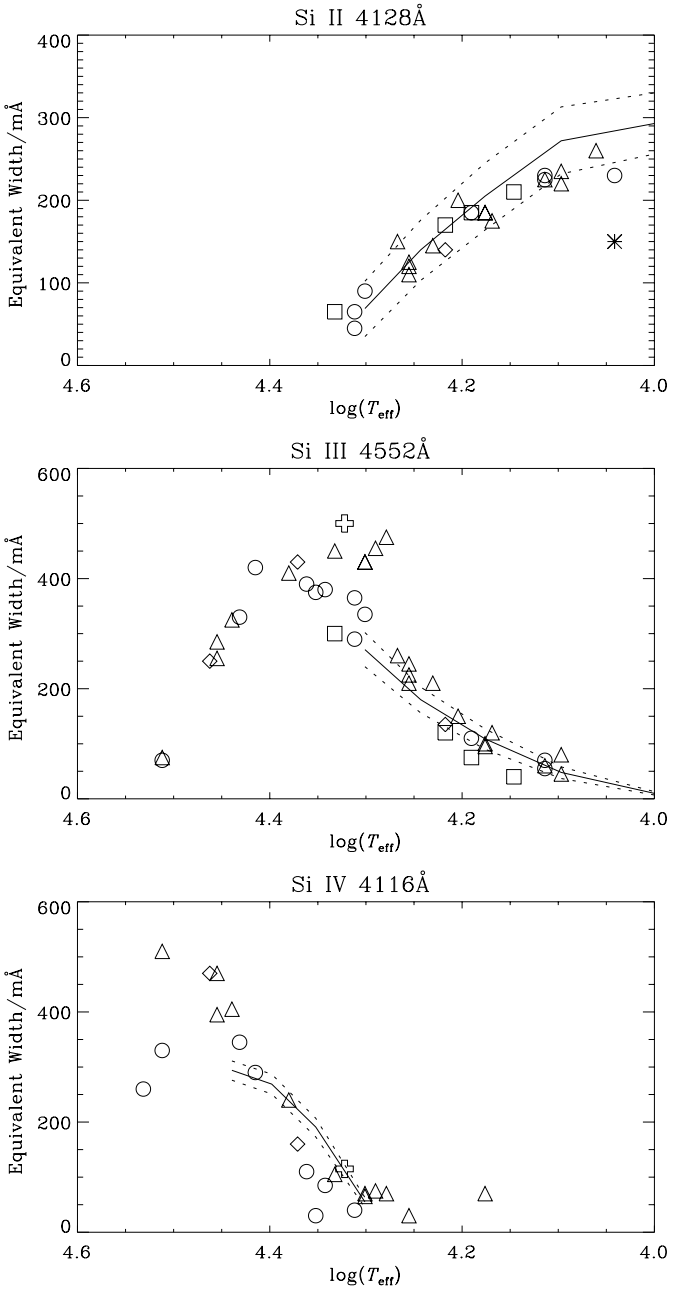

Fig. 5. Observed Si II/III/IV linestrengths compared with non-LTE predictions. The non-LTE loci are for silicon abundances of 7.28 dex ± 0.2 dex and $v_{\rm turb}$ = 10 km s^{-1}. The symbols are as in Fig. 2.

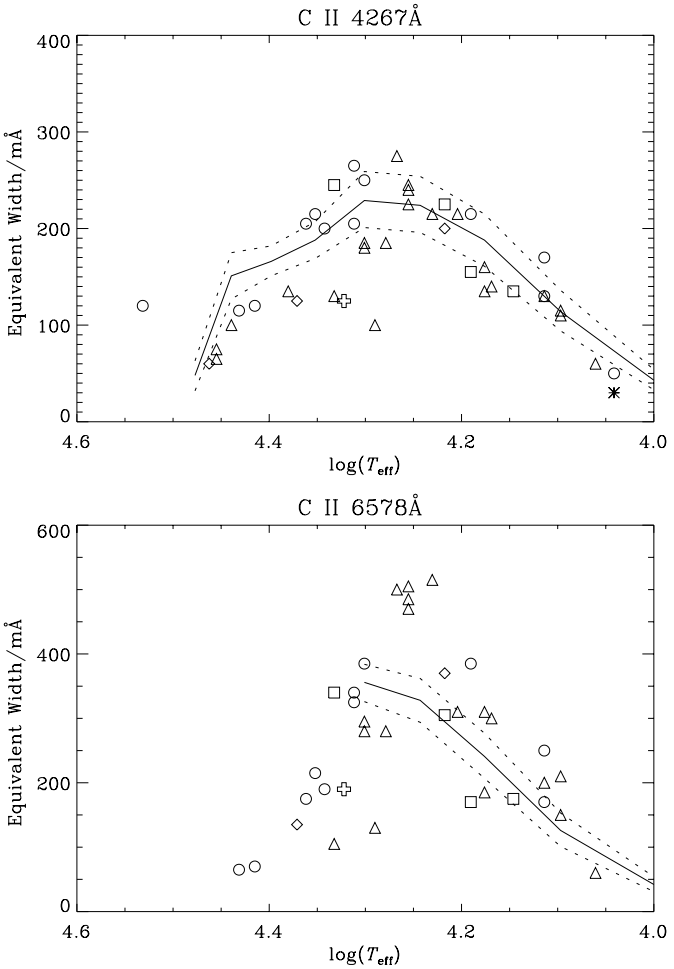

Fig. 6. Observed C II linestrengths compared with non-LTE predictions. The non-LTE loci are as follows: 4267 Å – [C/H]=7.80 and 6578 Å– [C/H]=8.20. Each plot shows predictions for $v_{\rm turb}$=10 kms^{-1} and includes loci at ±0.2 dex. The symbols are the same as those in Fig. 2.

note that the lines from the luminosity class II objects appear weaker than those of their more luminous counterparts. The agreement in abundance between Si II and Si III is expected due to the ionisation balances performed for these stars.

In the case of the Si IV feature at 4116 Å, the non-LTE locus is again restricted by problems in the computations. For effective temperatures above 27 500 K, the profiles are filled in or are entirely in emission. As was the case for some of the Si III profiles, we do not believe these effects to be real and suggest that they may again reflect our neglect of line blanketing. For the reduced range in effective temperature for which the silicon computations are believed to be realistic, the general behaviour of the 4116 Å feature is reproduced satisfactorily.

There is perhaps a suggestion that the 4116 Å feature indicates a slightly lower silicon abundance than the features due to Si III and Si II. However, when one notes the extreme luminosity sensitivity of the Si IV feature, coupled with the range in luminosities within the sample, it becomes difficult to confirm this. Certainly, to within the errors, all three silicon ionisation stages are consistent with a silicon abundance of approximately 7.28 dex, in excellent agreement with the results of Kilian.

6.3.3. Carbon

Paper II gave linestrength measurements for 3 C II features – the close doublet at 4267 Å, and the doublet components at 6578 & 6582 Å. We have elected to plot the equivalent widths of 4267 Å and of 6578 Å.

The feature at 4267 Å is the strongest C II feature in the classical blue region of B-type stellar spectra but is notoriously

difficult to model successfully. An early attempt to do so was made by Lennon (1983) whose non-LTE calculations overestimated the observed strength in main sequence B-type stars by a factor of two for a solar abundance. Later attempts by Eber & Butler (1988) and Sigut (1996), have increased the complexity of the model ion (notably by including quartet terms which were omitted by Lennon), and the latter paper demonstrates that the non-LTE line strengths have now converged with respect to model ion complexity. As can be seen from Fig. 6, our non-LTE calculations (which use the same atomic dataset as Eber & Butler) again overestimate the strength of the 4267 Å line for a normal B-type star abundance. However, for a reduced abundance of 7.80 dex, the *shape* of the distribution of linestrengths is satisfactorily reproduced. There are a number of supergiants which have linestrengths significantly less than their nearest neighbours in effective temperature. Whether this reflects variations in gravity or the carbon abundances in these stars will be discussed below.

The C II feature at 6578 Å is only satisfactorily modelled for effective temperatures below 20 000 K, with the hotter models predicting that this multiplet should be in emission. As this is not confirmed by the observations, we attribute this disagreement to a failing of our non-LTE computations for this multiplet at high effective temperature and note the similarity with the behaviour of some silicon features mentioned in Sect. 4.1. Again, large photoionisation rates and subsequent cascades are causing the emission and the lack of line-blanketing may mean our photoionisation rates are overestimated. It is however, interesting to note that the observed equivalent widths in the feature at 6578 Å do decrease sharply with increasing stellar effective temperature.

6.3.4. Nitrogen

Paper II gave linestrength measurements for 9 N II features which cover five multiplets. Three lines (at 3995, 4228 & 4447 Å) arise from transitions between singlet levels, with the others (at 4236 & 4241 and 4601, 4607, 4621 & 4630 Å) being from triplet levels.

We show in Fig. 7 linestrengths for the N II features at 3995, 4241, 4447 & 4630 Å, with the singlet and triplet N II features being shown on the left and right respectively. There is a qualitative difference in the behaviour of these two series, as the calculations of the singlet transitions exhibit a sharp increase in predicted linestrength at $\log T_{\rm eff} \sim 4.4$, which is absent from the triplet transitions. The cause of this discrepancy is unclear and it is not seen in the observed linestrength patterns.

We note that a normal B-type star nitrogen abundance of 7.69 dex provides satisfactory fits to the lower envelope of most of the observations. At effective temperatures below the 'bump' in the predicted singlet linestrengths, agreement is reasonable. In the case of the triplet features, the non-LTE predictions fit the observed lower envelope reasonably well throughout the temperature range.

The tendency for most of the observed linestrengths to lie above the non-LTE locus is contrary to the behaviour of the C II features, while the particularly large spread in linestrength at $\log(T_{\rm eff}) \sim 4.3$ mirrors the behaviour of the C II features. These effects may be due to differing nitrogen abundances across our stellar sample and this will be discussed further below.

6.3.5. Oxygen

Paper II gave linestrength estimates for 11 O II spectral lines covering 4 multiplets. In Fig. 8 we show one representative feature from each multiplet, namely the lines at 4075, 4317, 4596 & 4661 Å. The feature at 4596 Å is between doublet levels, whilst the rest are for quartet levels. For the latter, the general shape of the observed linestrengths is reproduced satisfactorily. In the case of the doublet feature at 4596 Å the agreement between theory and observation is limited to temperatures below $\log T_{\rm eff} \sim 4.3$ and this behaviour is replicated by the other line of this multiplet at 4590 Å. Hence we conclude that our computations do not successfully model this multiplet and again there is a discrepancy between the different spin series.

The effect of increasing the microturbulence to 20 km s^{-1}, whilst retaining a normal oxygen abundance is shown by the grey shaded areas. It appears that a $v_{\rm turb}$ >10 km s^{-1} may be appropriate for the oxygen lines, in agreement with other studies (MLD, Vrancken 1998), where a higher microturbulent velocity was estimated from lines of O II.

7. Evidence for chemical peculiarities

As was outlined in the introduction, photospheric chemical peculiarities due to the presence of core-processed material are predicted by current evolutionary theories (the precise amount of mixing varying markedly between different models). CNO-cycled material would be expected to have increased helium and nitrogen abundances, accompanied by decreased carbon and oxygen abundances, with the changes in carbon and nitrogen being the largest. These patterns are observed in the linestrengths of our supergiant sample; Figs. 6 and 7 show very large ranges in observed equivalent widths due to C II and N II, with Fig. 8 showing only moderate ranges for O II, while no significant variations within the helium linestrengths are apparent.

7.1. Identification of chemically diverse groups

It will be useful for the discussions below, to identify those stars which may have contaminated photospheres. Fig. 9 shows the ratios of equivalent widths of the N II line at 4630 Å to those of the C II line at 4267 Å. These features have been selected as they have reliable linestrength measurements, while their general behaviour as a function of effective temperature also appears to be reasonably well modelled by our non-LTE computations. In producing this figure, we have not used the equivalent widths tabulated in Paper II, but rather have remeasured the spectral features from the original data in order to try and improve the accuracy and also to obtain formal measurement errors. Also shown are the theoretical values of this ratio for a normal nitrogen abundance, a carbon abundance [C/H] = 7.80 dex (see

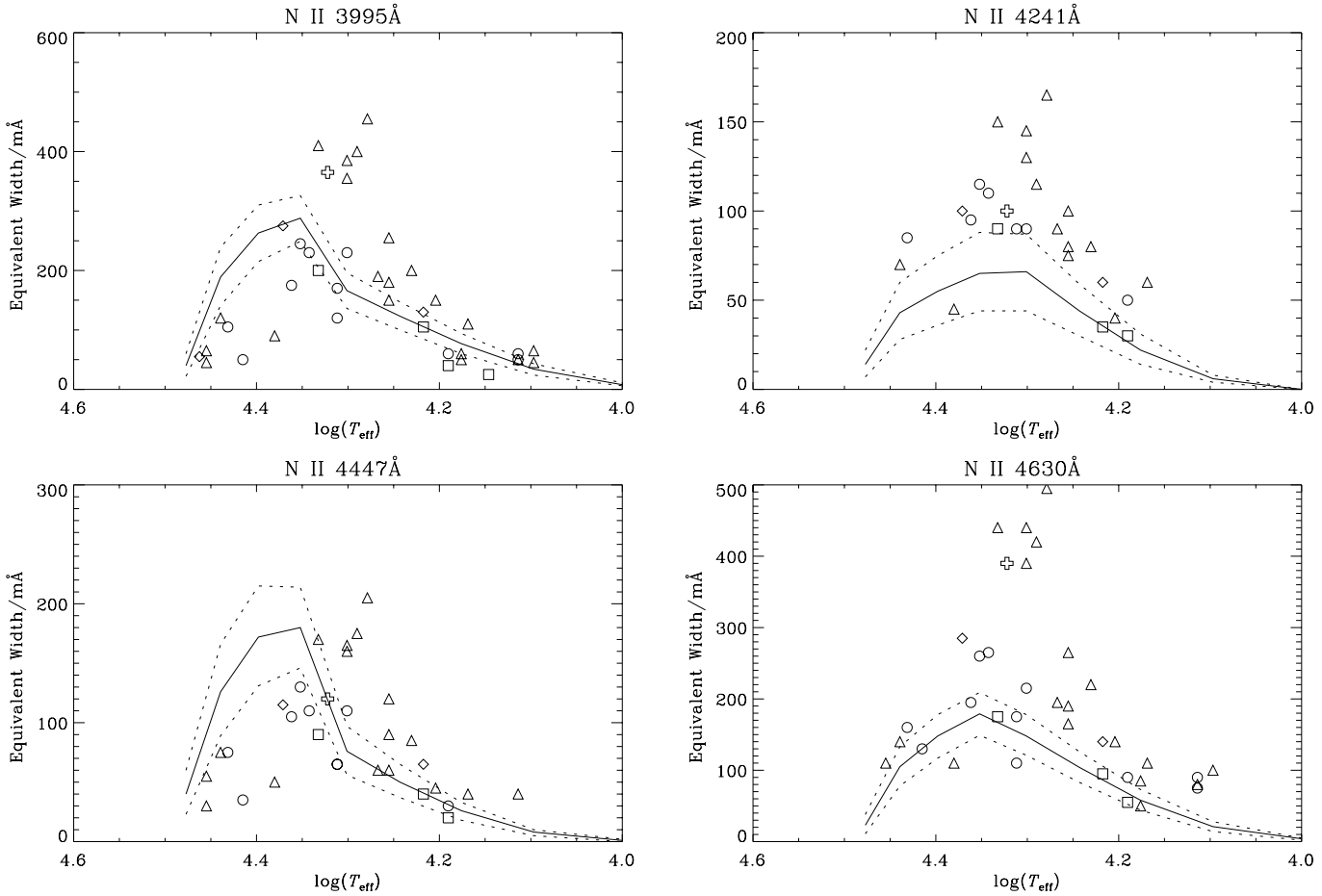

Fig. 7. Observed N II linestrengths compared with non-LTE predictions. Each plot shows predictions for[N/H] = 7.49, 7.69, 7.89 dex and for $v_{\rm turb}$ = 10km s^{-1}. The features shown on the left are singlets, whilst those on the right are triplets. There are clearly problems in modelling the singlets – see text for further discussion. The symbols are the same as those in Fig. 2.

Sect. 6.3.3) and a microturbulence of 10 km s^{-1}. As the luminosity dependence of the spectral lines may be important, the figure includes three non-LTE loci – the central curve is the ratio of predicted linestrengths for the $T_{\rm eff}$-log g relationship discussed in Sect. 6.1, while the dashed curves represent changes of $\pm$ 0.2 dex in log g. The relatively small displacements of these loci indicate that the luminosity effect cannot directly account for the observed linestrength patterns (note that some of the small structure in these loci may not be real but rather reflect the use of relatively simple interpolation techniques).

Three sub-groups can be tentatively identified in Fig. 9:

- supergiants that appear chemically near-normal (labelled 'normal/moderate' and lying close to our theoretical ratios)
- supergiants that appear to have had their photospheres contaminated by the products of CN-cycle burning (labelled 'highly processed' and lying away from the normal loci)
- supergiants which may have suffered from some contamination, but perhaps of a smaller magnitude (labelled 'processed?').

This figure, however, does not include the possibility of varying line desaturation due to, for example, a luminosity-dependent microturbulence, or a strong stellar wind. In this context, it is interesting to note that *all* the 'highly processed' supergiants have strong P Cygni Hα profiles, which would suggest that mass loss may play a role in the line formation. Nevertheless, whilst line desaturation could perhaps explain the increased N II linestrengths, it seems unlikely that such phenomena could explain the correlated weaknesses of some of the C II features.

The effective temperatures of the seven 'highly processed' supergiants lie between 19000 to 23500 K and in this range, there are also seven 'normal/moderate' supergiants. For the latter, the lines strengths of the C II line at 4267 Å and the N II line at 4630 Å are reasonably tightly bunched with mean value of 224 ± 25mÅ and 217 ± 24mÅ respectively. For the 'highly processed' group, the mean line strengths are 150 ± 35mÅ (C II) and 422 ± 65mÅ (N II); the larger standard deviations, particularly for the nitrogen line, possibly implies that this is not a chemically homogeneous group. Although the observational data do not warrant an analysis of the individual stars, we have attempted to estimate the differences in the carbon and nitrogen abundances between the two groups of objects. We have assumed a representative effective temperature of 21000 K, with a logarithmic gravity of 2.5 dex (see Fig. 2) and a microturbulent

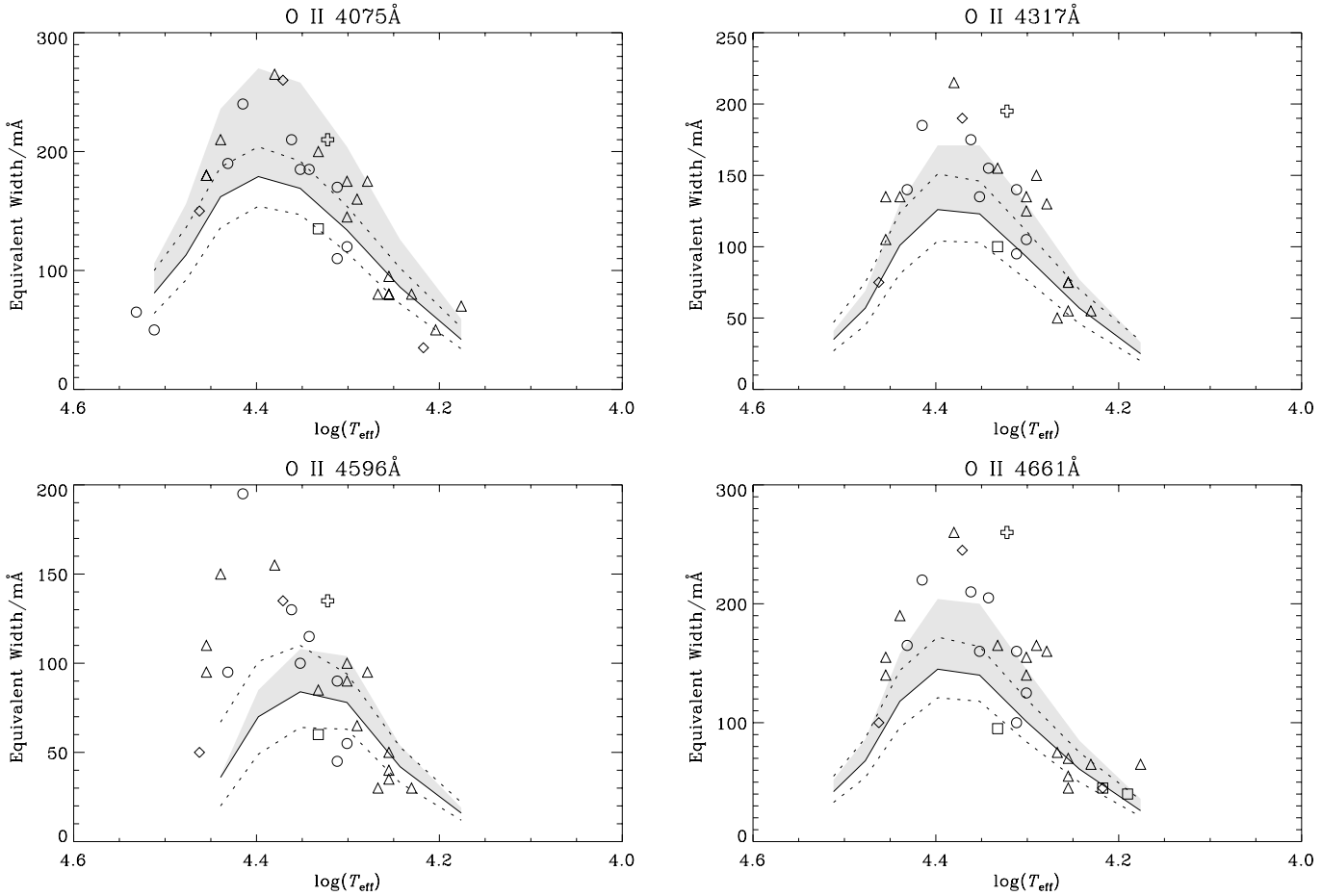

Fig. 8. Observed O II linestrengths compared with non-LTE predictions. Each plot shows predictions for [O/H] = 8.35, 8.55 & 8.75 dex and for $v_{\rm turb}$ = 10 km s^{-1}. The shaded area shows the effect of increasing $v_{\rm turb}$ to 20 km s^{-1} for an abundance of 8.55 dex. The symbols are the same as those in Fig. 2.

velocity of 10 kms^{-1}. The mean equivalent widths then imply that the 'highly processed' group are enhanced in nitrogen by 1.4 dex and depleted in carbon by 0.5 dex.

However, we emphasize that these results must be treated with considerable scepticism as they are subject to large uncertainties. For example, if the microturbulent velocity is increased to 15 kms^{-1}, the nitrogen enhancement is decreased to 0.9 dex. Additionally as discussed above, the 'highly processed' targets might have a larger microturbulence than the 'normal/moderate' targets; arbitrarily adopting microturbulent velocities of 15 kms^{-1} for the former and 10 kms^{-1} for the latter would further reduce the nitrogen enhancement to 0.6 dex. Although these calculations should be considered as numerical experiments, they illustrate that any quantitative estimate of abundance variations are critically dependent on the theoretical assumptions. Hence we can only conclude that the 'highly processed' targets probably exhibit a significant nitrogen enhancement coupled with a smaller carbon depletion (relative to the 'normal/moderate' group) and that this is consistent with nuclear processed material being present in their atmospheres.

7.2. Evidence for evolutionary patterns in oxygen and helium

It has already been shown above that variations in the abundance patterns of O II and He I within the supergiant sample are not obvious. This is consistent with the predicted changes in these element abundances and also their sensitivity to other parameters, such as the microturbulence and gravity. However, having used the more sensitive lines of carbon and nitrogen to identify apparently normal and processed groups within the sample, it is worthwhile reconsidering the linestrength patterns of oxygen and helium in this context.

In Figs. 10 and 11 we reproduce, for representative lines of He I and O II, the linestrength plots of Sect. 6. Only those objects which have been assigned to one of the 3 sub-groups are included in these figures. For helium, no obvious correlation between assigned chemical sub-group and the strengths of the lines is apparent. In the case of oxygen, the highly processed supergiants (which tend to be the most luminous) seem to show stronger oxygen features than the chemically normal supergiants. This is opposite to the trend expected from evolutionary considerations and may be due to a positive dependence

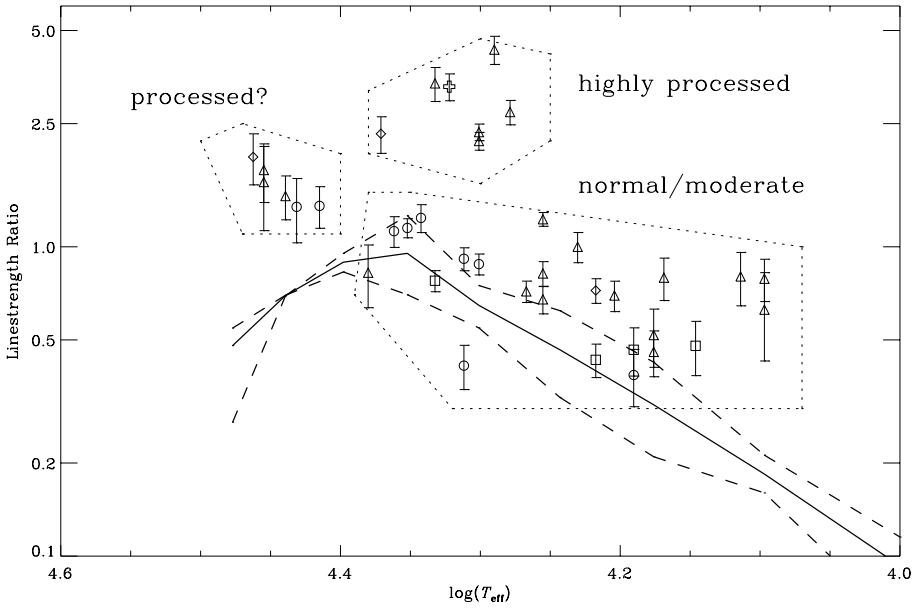

Fig. 9. Logarithmic ratios of equivalent widths for the lines at 4630 Å (N II) and 4267 Å (C II). The errors reflect uncertainties in the linestrength measurements. The non-LTE loci assume $v_{\rm turb}$ = 10 km s^{-1}, a solar helium fraction and [N/H] = 7.69 & [C/H] = 7.80 dex. Three predicted non-LTE ratios are shown, viz. that for the $T_{\rm eff}$-log g relationship shown in Fig. 2 (solid line) and two having the log g-scale displaced by $\pm$0.2 dex.

of microturbulence on luminosity, particularly as the value, derived from lines of O II, is very high for these luminous objects.

It is, therefore, not possible to derive quantitative information on the abundances of helium or oxygen from these plots. A more rigorous examination of the linestrength patterns, which allows for the effects of gravity and microturbulence, must be performed in order to elucidate any evolutionary patterns in these lines.

8. Discussion

8.1. Validity of the non-LTE calculations

Figs. 3 to 8 show that, whilst problems remain, the hydrostatic non-LTE modelling used in this analysis can satisfactorily reproduce the optical spectra of B-type supergiants. The low gravities of some of the models have, however, led to difficulties in synthesising some spectral features - most notably, the He I triplet transitions, N II singlet transitions at high effective temperatures, the O II doublet transitions, and Si III triplet transitions at high effective temperatures and low gravities. Problems were also encountered in reproducing the strength of the C II feature at 4267 Å. However, this feature is difficult to model even in main sequence B-type stars (Eber & Butler 1988, Sigut 1996), and therefore the problems are not unique to our low gravity models. An exhaustive investigation into the reasons for these shortcomings has not been performed. However, the fact that the problems are often localised to the hotter models having low gravities and that photoionisation rates are extremely high in these models is highly suggestive of a problem in calculating the UV radiation field. The lack of metal line blocking in our model atmosphere calculations will lead to an overestimation of the radiation field and a first step towards the possible resolution of these problems would be the inclusion of some form of increased line-blanketing. Recent attempts at including metal line-blanketing within non-LTE models have been discussed by, for example, Hubeny et al. (1998).

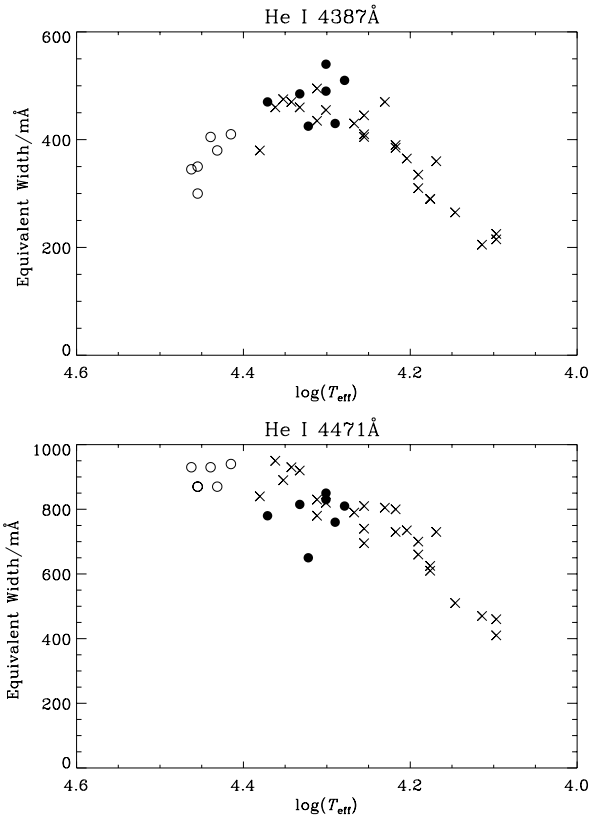

Fig. 10. Measured He I linestrengths for representative features at 4387 and 4471 Å. The symbols represent the CN status of the supergiants as follows: cross – 'normal/moderate', open circle – 'processed?', filled circle – 'highly processed'.

The spectral features, which are not satisfactorily modelled, are often between levels, that are not radiatively coupled to the

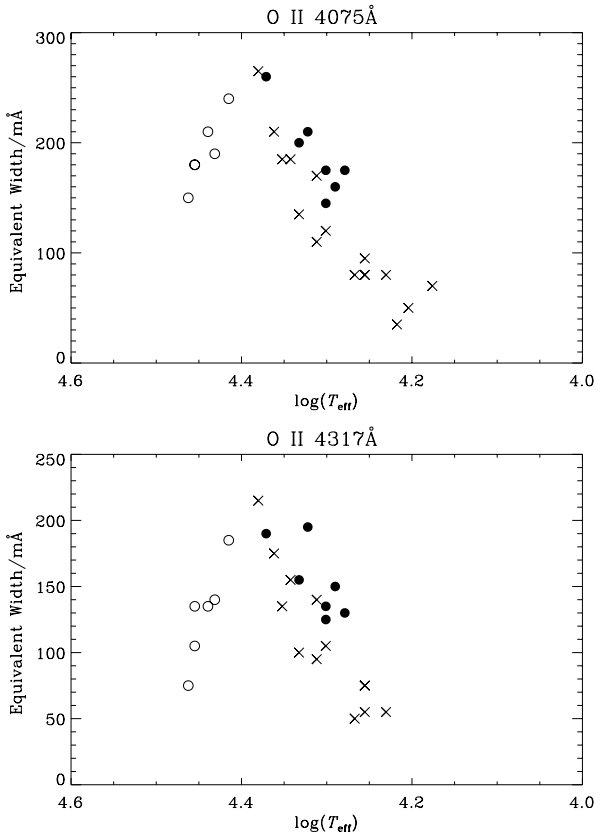

Fig. 11. Measured O II linestrengths for representative features at 4075 and 4317 Å. The symbols are the same as in Fig. 10.

atomic or ionic ground state. So, for example, the singlet lines of neutral helium are better modelled than the triplets. It is also interesting to note that the only lines of Si III observed here are triplets (Si III has a singlet ground state) and that this may explain the difficulties encountered in the modelling. Unfortunately, the spectral data are not good enough to reliably measure any singlet Si III features, such as that at 4717 Å.

Hence, we recommend that when using unblanketed non-LTE models (particularly for hot, low gravity stars) greater weight is given to transitions that are radiatively connected to the appropriate ground state.

8.2. Microturbulence

It would appear that a non-zero value for the microturbulence parameter is required to reproduce the linestrengths in *all* atomic species. Whilst the errors associated with the estimation of atmospheric parameters are large, and systematic effects (e.g. variations of $v_{\rm turb}$ with chemical species) may be present, the requirement of a non-zero value is an interesting result, which supports the findings of numerous other authors (see references in Sect. 5.3). It is possible that mass loss (Lamers & Achmad 1994, Kudritzki 1992) may have a role in desaturating the lines in these luminous objects, although, from the analysis presented here, it is difficult to draw any useful conclusions. It is however, interesting to note that whilst supergiants have systematically higher microturbulences than are typically adopted for their main sequence counterparts (5 km s^{-1} is often used – see, e.g., Smartt et al. 1996a and references therein), there is no evidence for any systematic difference in $v_{\rm turb}$ between the Ib and Ia supergiants.

8.3. Helium fractions, y

The findings of MLD – namely that the use of a non-zero microturbulence can lead to *near-normal* helium fractions in early B-type supergiants – is confirmed here, for the whole range of B-type supergiants. This is an important result as previous authors had found large helium fractions in many luminous OB-stars (see MLD and references therein). Additionally these results support our use of a normal helium abundance when deducing the atmospheric parameters. However, the moderate quality of our spectroscopic data does not preclude the possibility that our some of our sample may have moderate helium enhancements.

8.4. CNO abundances and stellar evolution

Fig. 12 shows the location of the supergiants in the $T_{\rm eff}$-$\log g$ plane, along with the solar metallicity evolutionary tracks of Schaller et al. (1992). These tracks do not include effects due to stellar rotation, which may be important (see Sect. 8.5). However with this limitation, they constitute a complete and consistent theoretical grid and hence form a useful basis for comparison with our observations. Only the B-type supergiants, that have been assigned a CN status are included in the figure – hence the 3 hottest and 5 coolest objects have been omitted.

Also shown in Fig. 12 are a sample of B-type (near) main sequence stars taken from Gies & Lambert (1992) and Kilian (1992) and a sample of A-type supergiants from Venn(1995a). For the main sequence stars, both studies implied that in general the atmospheric CNO abundances were normal apart from a few cases where there was evidence for moderate degrees of nuclear processing. The relationship between the A-type supergiants and their apparent progenitors, the B-type dwarfs, has been discussed in detail by Venn (1995b), who found that the [N/C] ratios of her supergiants were in general larger than those of the dwarfs, but less than the post-First Dredge-Up ratio predicted by evolutionary models. Hence, she concluded that her supergiants were pre-RSG objects which had suffered partial mixing during their main-sequence lifetimes.

There are a number of important caveats, which must be considered before any interpretation can be made of Fig. 12. Firstly, Gies & Lambert (1992) and Venn (1995a) used the model atmosphere structures of Kurucz (1991), and hence offer effective temperatures on an LTE, line-blanketed scale. Kilian (1992) used the model atmospheres of Gold (1984), which also include some blanketing. Therefore, their temperatures estimates are likely to be reasonably internally consistent but will differ from our scale based on unblanketed models. Hence the temperature scale for our B-type supergiants has been uniformly reduced by 10 % to allow for the effects of line blanketing as discussed in Sect. 6.1. Secondly, the estimation of gravity may

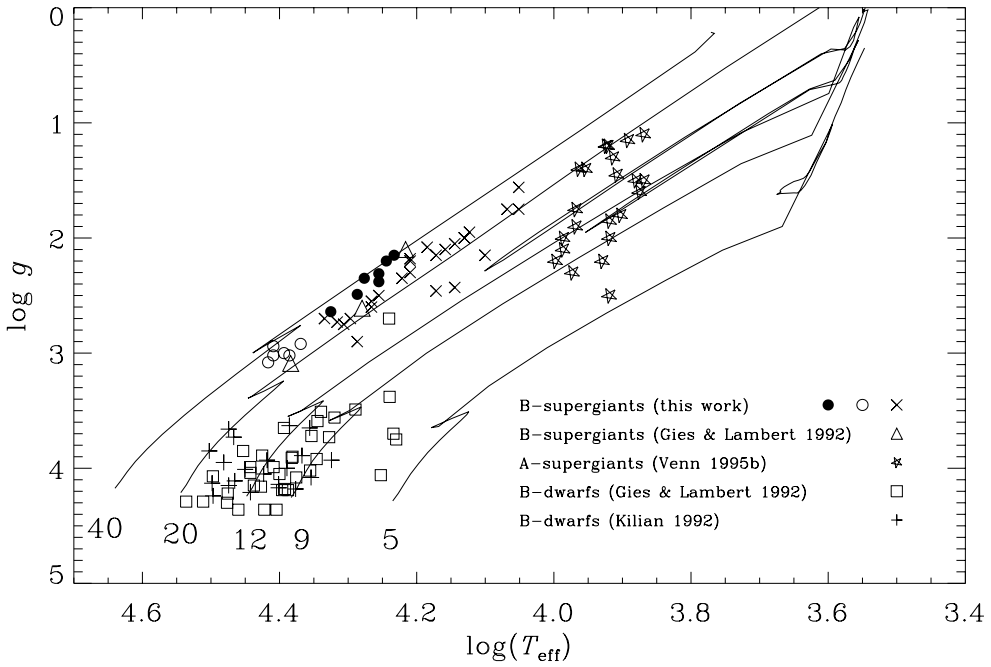

Fig. 12. The positions of the B-type supergiants, and some comparison objects, in the $T_{\rm eff}$-log g plane. The symbols are summarized in the figure, with • indicates 'highly processed', ○ 'processed?' and × 'moderate/normal' – see text for further discussion. Also shown are the evolutionary tracks of Schaller et al. (1992) together with their ZAMS masses. Note the $T_{\rm eff}$-scale for the B-type supergiants has been uniformly reduced by 10 % to account for their expected offset relative to the other objects

be subject to errors due to the modelling assumptions made. Specifically, neglecting the dynamic effects of mass loss and also line-blanketing can lead to underestimates (see Gabler et al. 1989 and Lanz et al. 1996, respectively), with the effects likely to be greatest for the more luminous supergiants.

The principal implications from Fig. 12 are as follows

- There appears to be a mass segregation between the 'highly processed' and 'normal/moderate' B-type supergiants, with the former lying on the higher mass evolutionary tracks. The hotter supergiants, designated as 'processed?', also lie on higher mass tracks.
- Practically all our B-type supergiants appear to be evolutionary distinct from either the B-type dwarfs or the A-type supergiants. The evolutionary calculations imply that their main sequence precursors would be O-type, whilst they would evolve into higher luminosity A-type supergiants than the predominantly Ib class discussed by Venn (1995b). A small number of our targets (approximately four) are on similar evolutionary tracks to the B-type main sequence and A-type supergiant stars but these all have approximately normal CNO abundances consistent with the other two samples.

Assuming that the non-rotating, single object, evolutionary tracks of Schaller et al. (1992) are appropriate, a possible evolutionary scenario to explain the observed abundance patterns would be as follows. Mixing has occurred on or near the main sequence and is strongly and positively correlated with the stellar mass. Then our lower mass B-type supergiants have suffered little or no atmospheric mixing and have retained near-normal surface compositions. These objects will eventually evolve into A-type supergiants, similar to those analysed by Venn (1995b). Although she found moderate CN anomalies, such relatively small chemical variations could be present within our 'normal/moderate' stellar group but be masked by the quality of our observational data. The hotter 'processed?' supergiants would then be the progenitors of the 'highly processed' supergiants and significant changes in surface chemistry would be occurring in a short period of time (Schaller's computations suggest that the evolution from $T_{\rm eff} \simeq 4.65$ to $T_{\rm eff} = 4.25$ – i.e. from the the main sequence to the 'highly processed' group – takes approximately 4.3 million years for a 40 $M_{\odot}$ model). However, it should be noted that the hotter 'processed?' stellar sub-group lies in an effective temperature range for which there are difficulties in the modelling computations. Hence, it is possible that for these stars, the apparent surface chemical effects may simply be an artefact of our analytical approach.

8.5. Alternative evolutionary scenarios - rotation and binarity

As was discussed in the introduction, stellar rotation may have a role to play in the chemical mixing of stellar atmospheres. Massive main sequence stars are rapid rotators, having equatorial velocities of up to 400 km s^{-1} (Penny 1996, Howarth et al. 1997) and these may be large enough to cause significant mixing in their atmospheres due to the effects of differential rotation and the subsequent instabilities which are introduced. They may also cause significant changes in the stellar evolutionary tracks themselves – even during the main sequence phase.

Fig. 13 shows the dependence of projected rotational velocity, $v \sin i$, on effective temperature. The $v \sin i$ values are taken from Howarth et al. (1997) and omit a number of the B-type supergiants considered here, most notably the 'highly processed' stars HD 14956 & HD 194279. However, the $v \sin i$ values estimated here (see Table 1) for these objects (75 & 70 km s^{-1} respectively) would put them in a similar position to the other 'highly processed' supergiants. Despite the small number statistics, the 'highly processed' supergiants appear, on

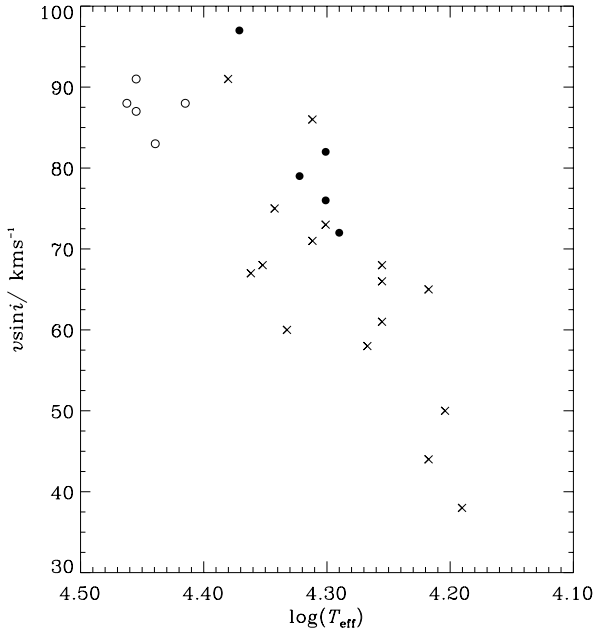

Fig. 13. The figure shows the projected rotational velocity, $v \sin i$, as a function of effective temperature for some of the B-type supergiant sample. The 'highly processed' stars clearly have larger $v \sin i$ values than the 'normal/moderate' objects. The symbols represent the CN status of the supergiants as follows: $\times$ – 'moderate/normal', $\circ$ – 'processed?', $\bullet$ – 'highly processed'.

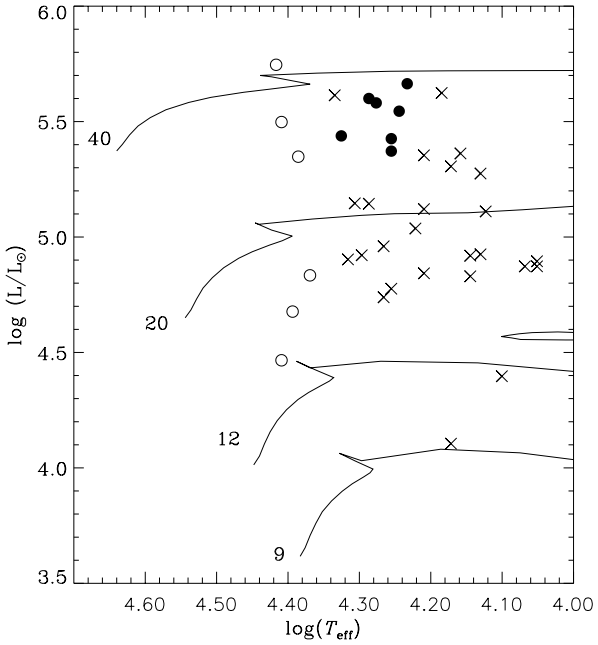

Fig. 14. The positions of the B-type supergiants in the $T_{\rm eff}$-$L/L_\odot$ plane. The $T_{\rm eff}$-scale for the B-type supergiants has been uniformly reduced by 10%. The stellar luminosities are taken from Lennon (1994). The evolutionary tracks of Schaller et al. are shown, along with their ZAMS masses. The differing chemical sub-groups are plotted using the same symbols as in Fig. 12.

average, to have larger projected rotational velocities than the 'normal/moderate supergiants' and could imply a connection between chemical mixing and stellar rotation rate.

However the projected rotational velocities estimated by Howarth et al. are observational parameters which may correlate with but are unlikely to equate to the physical projected equatorial rotational velocity. For example, other physical mechanisms, such as macroturbulence, may contribute to the observed broadening; then the greater line broadening in the 'highly processed' group could simply reflect their higher luminosities and hence greater atmospheric macroturbulence. Indeed as discussed by Howarth et al., the absence of early-B-type supergiants with low projected rotational velocities indicates that another broadening mechanism (as well as rotation) must be present. Hence we conclude that there is some evidence for our 'highly processed' supergiants having broader spectral lines but it is unclear whether this is a signature of enhanced rotational velocities.

In Fig. 14, the positions of our B-type supergiants in the $T_{\rm eff}$-$\log(L/L_\odot)$ plane are shown (see Sect. 2 for sources of luminosity estimates).

It is notable that the stellar masses in Figs. 12 and 14 are not coincident. This is a manifestation of the well-known mass discrepancy problem (see, e.g. Herrero et al. 1992), whereby stellar masses derived from non-LTE spectroscopic methods and those based on evolutionary calculations, typically do not agree. Specific areas which may lead to a resolution of this discrepancy are improvements in the calculation of gravities (e.g. using hydrodynamic atmosphere codes) and proper treatment of line blocking effects (Lanz et al. 1996). However, the discrepancy is not crucial to this discussion as Fig. 14 supports the broad conclusions drawn from Fig. 12 – namely that the two sub-groups which appear to have processed material in their atmospheres are generally more massive than the chemically normal supergiants.

An uncertain fraction of luminous stars may be members of binary or indeed multiple systems. In the case of close binaries, interactions may occur which have a very important effect on the evolution of the individual stars. Mass transfer is predicted between the components and the changing stellar masses lead to complex changes in the evolutionary tracks. Langer et al. (1999) have recently considered the evolution of a close 20 + 18 $M_\odot$ pair, where mass transfer during the core hydrogen burning phase of the primary is included. They have shown that the primary in such a system may evolve into a helium star while the secondary may evolve into a luminous blue supergiant – such as is considered here. During the main sequence lifetime of the primary, mass transfer leads to a deposition of helium enriched matter onto the surface of the secondary. This generates an inversion in the mean molecular weight gradient in the secondary and leads to significant atmospheric mixing (so-called thermohaline mixing) with changes in the abundances of carbon and nitrogen, by factors of 2–3, being predicted. Although these are smaller than the values estimated in Sect. 7.1, the uncertainties in these estimates are such that they may well be consistent with the predictions. The evolutionary calculations also imply

that during the accretion of the extra mass, the luminosity of the secondary may increase substantially. In the case of their 18 $M_{\odot}$ (ZAMS) object, Langer et al. predict that after the mass transfer, $\log(L/L_{\odot}) \sim 5.4$–$5.5$ and $\log(T_{eff}) \sim 4.3$–4.5; both consistent with the position of our 'highly processed' group of B-type supergiants. Clearly, their calculations are preliminary and need to be extended to include other initial masses. However, binarity is clearly an important evolutionary mechanism which may reproduce the observed abundance patterns in some supergiants, including our 'highly processed' group.

Acknowledgements. We would like to thank Rolf Kudritzki, Kim Venn, Norbert Langer, Robert Rolleston and Robert Ryans for many useful discussions. This work has made use of model atmosphere programs made available through the PPARC supported Collaborative Computational Project No. 7. NDME would like to acknowledge financial support from the Department of Education for Northern Ireland, while DJL is grateful for support from the Bundesminister für Forschung und Technologie under grant 010 R 90080. We are grateful to the British Council and the Akademischer Austauschdienst for funding an ARC program of working visits between Munich and Belfast.

References

Barlow M.J., Cohen M., 1977, ApJ 213, 737
Becker S.R., Butler K., 1988, A&A 201, 232
Becker S.R., Butler K., 1989, A&A 209, 244
Becker S.R., Butler K., 1990, A&A 235, 326
Becker W., Fenkart R., 1971, A&AS 4, 241
Brown A.G.A., Blaauw A., Hoogerwerf R., de Bruijne J.H.J., de Zeeuw P.T., 1999, astro-ph/9902234
Butler K., 1984, Ph.D. Thesis, University of London
Crowther P.A., 1997, In: Beddings T.R., Booth A.J., Davis J. (eds.) Proceedings of IAU Symp. 189, Fundamental Stellar Properties: The Interaction between Observation and Theory. Kluwer, p. 137–146
Cunha K., Lambert D., 1992, ApJ 399, 586
Cunha K., Lambert D., 1994, ApJ 426, 170
Denissenkov P., 1994, A&A 287, 113
Eber F., Butler K., 1988, A&A 202, 153
ESA, 1997, The Hipparcos and Tycho Catalogues. ESA SP-1200
Fitzpatrick E.L., Bohannan B., 1993, ApJ 404, 734
Gabler R., Gabler A., Kudritzki R.-P., Puls J., Pauldrach A., 1989, A&A 226, 162
Giddings J.R., 1981, Ph.D. Thesis, University of London
Gies D.R., Lambert D.L., 1992, ApJ 387, 673
Gold M., 1984, Diplomarbeit Universität München
Herrero A., Kudritzki R.-P., Vilchez J.M., et al., 1992, A&A 261, 209
Hibbins R.E., Dufton P.L., Smartt S.J., Rolleston W.R.J., 1998, A&A 332, 681
Howarth I.D., Siebert K.W., Hussain G.A.J., Prinja R.K., 1997, MNRAS 284, 265
Hubeny I., 1988, Computer Physics Comm. 52, 103
Hubeny I., Heap S.R., Lanz T., 1998, In: Howarth I.D. (ed.) Boulder-Munich II: Properties of Hot, Luminous Stars. ASP Conf. Series Vol. 131, ASP, San Francisco, p. 108
Humphreys, R.M., McElroy, D.B., 1984, Catalogue of stars in stellar associations and young clusters. Univ. of Minnesota.
Jaschek M., Jaschek, M., 1967, ApJ 150, 355
Kilian J., 1991, A&A 244, 419
Kilian J., 1992, A&A 262, 171
Kilian J., 1994, A&A 282, 867
Kudritzki R.-P., 1992, A&A 266, 395
Kurucz R.L., 1979, ApJS 40, 1
Kurucz R.L., 1991, In: Philip, Upgren, Janes (eds.) Precision Photometry: Astrophysics of the Galaxy. L. Davis Press, Schenectady
Lamers H.J.G.L.M., 1981, ApJ 245, 593
Lamers H.J.G.L.M., Achmad L., 1994, A&A 291, 856
Langer N., Maeder A., 1995, A&A 295, 685
Langer N., Heger A., Braun H., 1999, Nucleosynthesis in Massive stars. In: Mezzacappa T. (ed.) Atomic and Nuclear Astrophysics. Proc. 2nd. Oak Ridge Symposium, IOP publishing, 377
Lanz T., de Koter A., Hubeny I., Heap S.R., 1996, ApJ 465, 359L
Lennon D.J., 1983, MNRAS 205, 829
Lennon D.J., 1994, Space Sci. Rev. 66, 127
Lennon D.J., 1997, A&A 317, 871
Lennon D.J., Dufton P.L., 1989, A&A 225, 439
Lennon D.J., Dufton P.L., Keenan F.P., Holmgren D.E., 1991a, A&A 246, 175
Lennon D.J., Kudritzki R.-P., Becker S.R., et al., 1991b, A&A 252, 498
Lennon D.J., Dufton P.L., Fitzsimmons A., 1992, A&AS 94, 569
Lennon D.J., Dufton P.L., Fitzsimmons A., 1993, A&AS 97, 559
Lester J.B., Gray R.O., Kurucz R.L., 1986, ApJS 61, 509
Maeder A., Conti P.S., 1994, ARA&A 32, 227
Maeder A., Meynet G., 1989, A&A 210, 155
Massey P., Johnson K.E., DeGioia-Eastwood K., 1995, ApJ, 454, 151
McErlean N.D., Lennon D.J., Dufton P.L., 1998, A&A 329, 613
Mermilliod J.-C., Mermilliod M., Hauck B., 1997, A&AS 124, 349
Mihalas D., 1972, ApJ 177, 115
Nicolet B., 1981, A&A 104, 185
Penny L.R., 1996, ApJ 463, 737
Rupprecht J., 1966, Trans. IAU 12B, 350
Schaller G., Schaerer D., Meynet G., Maeder A., 1992, A&AS 96, 269
Schönberner D., Herrero A., Becker S., et al., 1988, A&A 197, 209
Sigut T.A.A., 1996, ApJ 473, 452
Smartt S.J., 1996, Ph.D. Thesis, The Queen's University of Belfast
Smartt S.J., Dufton P.L., Rolleston W.R.J., 1996a, A&AS 116, 483
Smartt S.J., Dufton P.L., Rolleston W.R.J., 1996b, A&A 310, 123
Smartt S.J., Dufton P.L., Lennon D.J., 1997, A&A 326, 763
Smith K.C., Howarth I.D., 1994, A&A 290, 868
Smith K.C., Howarth I.D., 1998, MNRAS 299, 1146
Talon S., Zahn J.-P., Maeder A., Meynet G., 1997, A&A 322, 209
Tuchman Y., Wheeler J.C., 1990, ApJ 363, 255
Venn K.A., 1995a, ApJS 99, 659
Venn K.A., 1995b, ApJ 449, 839
Voels S.A., Bohannan B., Abbott D.C., Hummer D.G., 1989, ApJ 340, 1073
Vrancken M., 1998, Ph.D. Thesis, Vrije Universiteit Brussel
Walborn N.R., 1972, AJ 77, 312
Walborn N.R., 1976, ApJ 205, 419
de Zeeuw P.T., Hoogerwerf R., de Bruijne J.H.J., Brown A.G.A., Blaauw A., 1999, AJ 117, 354
Zorec J., Briot D., 1991, A&A 245, 150